Chapter 13

Structure - Properties Interrelationships in Multicomponent Solutions Based on Cellulose and Fibers Spun Therefrom

Ludmila Golova, Igor Makarov, Ludmila Kuznetsova,
Elena Plotnikova and Valery Kulichikhin

Additional information is available at the end of the chapter

http://dx.doi.org/10.5772/51688

1. Introduction

Cellulose is a natural polysaccharide with a practically inexhaustible raw source. The unique properties of cellulose, such as biodegradability, excellent mechanical properties, and relatively high hydrophilicity, make it possible to manufacture household and industrial materials on its base, which are useful for various applications.

Owing to its structural features, the transition of cellulose to the plastic state presents a challenge. Cellulose decomposes prior to the onset of melting; therefore, dissolution is the only way of preparing spinning systems for fiber and film formation. However, the regular structure of cellulose macromolecules, the presence of a developed system of H-bonds, and a relatively high rigidity of chains (the Kuhn segment is ~100 Å) sharply confine the range of possible solvents for cellulose. Intensive studies conducted by many research and industrial groups have led to the discovery of a new class of nonaqueous solvents for cellulose: oxides of tertiary amines, and among them *N*-methylmorpholine-*N*-oxide (NMMO) was found to be the most efficient since can dissolve up to 20% cellulose [1-5].

Cellulose fibers processed via "MMO process" and referred to as Lyocell fibers according to the resolution by the BISFA, are characterized by their highly ordered structural organization (high degree of crystallinity and orientation). On the one hand, the strength and modulus of the resultant fibers are high; on the other hand, their deformation characteristics are low, and the tendency toward fibrillation exists. As a result, processing becomes more difficult and the service characteristics of fibers deteriorate.

This poses an extremely important problem which, despite the efforts of researchers from many countries has not been solved yet. What are the ways to efficiently govern the fibrillation of Lyocell fibers?

Obviously, this situation requires fundamentally new solutions for controlling the structuring in cellulose and, hence, for the optimization of Lyocell fibers characteristics.

In our opinion, controlling the process of the structure formation of cellulose macromolecules should be solved on micro-and nanolevels by means of creation of multicomponent solutions via introducing to cellulose solutions of polar polymers of different nature or layered anisometric nanoparticles of aluminosilicate with high interfaces and surface energy. The idea of this way consisted in appearance of hindrance at crystallization of cellulose in gel-fibers to decrease their capability to fibrillation.

The basis for solving the problem associated with the structure management of cellulose on micro- and nanolevels in mixed solutions containing cellulose and various synthetic polymers or aluminosilicates is a new method of solid-phase dissolution of cellulose in NMMO, which allows to improve significantly the dissolving ability using high-melting hydrate forms of NMMO and obtaining highly concentrated dopes with concentration of cellulose up to 40% [6-7].

The aim of ongoing research is to develop approaches for controlling the structure of cellulose fibers obtained from solutions in NMMO. In this connection, it has been a challenge to study in detail the efficiency of NMMO as a solvent with respect to hydrophobic synthetic polymers of various nature, to investigate the mutual dissolution of cellulose and synthetic polymers in NMMO, and to characterize the rheological characteristics and structure-morphological features of mixed solutions in order to identify the evolution in the structure of cellulose in all stages from dissolution to spinning of oriented fibers. We investigate the mechanical properties of hybrid fibers, which were selected as a criterion for the choice of regimes for the formation of desired structure for cellulose fiber nanocomposites. All these tasks have been considered in this Chapter.

2. Objects

Baikal softwood cellulose with a degree of polymerization of 600 containing 8% of water (this level corresponds to its equilibrium sorption under normal conditions) was used. As polymeric additives, polar linear thermotropic LC alkylenearomatic polyesters with mesogenic triads based on fumaric and oxybenzoic acids with hexa- (HP-6) and decamethylene (HP-10) spacers, CPEs with different content of repeating units of the parent homopolymers, and CPEs with mesogenic triads based on terephthalic and oxybenzoic acids and decamethylene (PDTOB) spacers were chosen. Along with LC polyesters, the solubility of the amorphous aromatic polyamide poly (*m*-phenyleneisophthalamide) (PMPIA) in NMMO was examined as well.

Dissolving systems were monohydrate NMMO (13.3% of water) and high-melting hydrate form of NMMO with T_m = 120–160°C (water content was 8–10%).

As to aluminosilicate particles, the majority of experiments were carried out with two kinds of clays: Na-montmorillonite (Cloisite Na^+) and montmorillonite treated with dioxydecyldimethylammonium chloride (Cloisite 20A) produced by Southern Clay Product, USA.

3. Methods

3.1. Preparation of solutions

Polymer solutions in high melting NMMO crystal hydrate were prepared by mixing of powder components in definite way and subsequent heating in laboratory reactor equipped with stirring device. A completeness of the dissolution was monitored visually or with polarizing microscope by measuring the temperature of system transition to the fully isotropic liquid state.

All joint solutions of cellulose with synthetic polymers in NMMO were prepared according to the following procedure: preliminary solid-phase activation of the cellulose–NMMO system, subsequent addition of synthetic polymer, and homogenization at heating of three-component mixture by mechanical stirring. To inhibit thermo-oxidative degradation of NMMO and cellulose, 0.5% propylgallate was added. Under simultaneous action of temperature and deformation (e.g. at passing through an MV-3M capillary viscometer at 120°C), solid-phase composite melts and passes to flow state. A completeness of all components dissolution in NMMO was controlled by optical observation.

An original method for preparing solid-phase compositions of cellulose with layered aluminosilicates Cloisite Na^+ and Cloisite 20A has been developed. The addition of clay to the previously obtained "solid" pre-solution of cellulose in NMMO provides a high dispersion and a uniform distribution of clay particles in a matrix cellulose phase. As soon as the system was additionally activated, solid-phase compositions containing 10, 14, and 18 wt% of cellulose, and Cloisite Na^+ or Cloisite 20Å in amounts from 0,1 to 20 wt% were obtained.

Since dimensions of particles in raw clay Cloisite Na^+ usually are equal to 3-7 mkm, a method of fractionation of them with extraction of nanodimensional particles by means of "aqueous activation/modification" by means of sedimentation and dynamic light scattering methods (centrifuge CPS 24000) the distribution curves were obtained. Choosing optimal regimes of aqueous activation and drying, particles of modified clay (M_2Cloisite Na^+) with dimensions 20-100 nm were prepared.

3.2. Research methods

The phase equilibrium and morphological features of polymer–NMMO systems were studied using Boetius polarization microscope (VEB Kombinat Nadema, former DDR).

DSC studies were performed on a Mettler 822e differential scanning calorimeter at a heating rate of 10 K/min.

X-ray measurements were carried out on DRON-3 and DRON-3M diffractometers (Ni-filtered CuK$_\alpha$ radiation) equipped with a high-temperature chamber (the temperature control allowed to keep accuracy within 1°C) and an IRIS-3.0 instrument (Ni-filtered CuK $_\alpha$ radiation, flat cassettes). Diffractograms and X-ray patterns of the samples were taken in the transmission mode.

The rheological characteristics of solutions were studied by MV-3M capillary viscometer of melt-indexer type and rotation rheometer PIRSP-2 steady-state and low-amplitude oscillation shear deformations using cone–plate operating unit. This equipment renders it possible to cover a wide interval of shear rates $\dot{\gamma}$ = 10^{-3}–10^{3} s^{-1} and shear stresses τ = 10–10^{6} Pa. The use of capillaries with different length, *L* to diameter, *D* ratio (5–40) showed that the correction for entrance effects is small (1.0–1.5) and for capillaries with high *L*/*D* ratio can be neglected. The viscosity of all systems was measured at 120°C. To visualize the flow morphology of solutions during deformation, the rotational rheometer was equipped with: (i) transparent plate–plate unit and glass optical windows, (ii) on a top plate the prism of full internal reflection was installed together with a polar (analyzer), and (iii) a lamp with a narrow focused light beam and polarizer was positioned in a hollow shaft of rheometer.

For estimation of the fibrillation capacity the obtained cellulose and hybrid fibers were treated in vibration mill M35L (oscillation amplitude is 4 mm, frequency is 48 Hz, power of electric engine is 1.7 kW) during 30 min in aqueous medium

Micrographs of composite materials on nanoscale were obtained using electron microscope LEO 912 AB OMEGA (Carl Zeiss, Germany) with a cathode based on LaB. The acceleration voltage is 100kV.

The tensile strength, the initial elastic modulus and elongation at break fibers and extrudates under consideration were measured with Instron 1122 testing machine at elongation rate of 10 mm / min.

4. Results and discussion

4.1. Crystal solvates of thermotropic alkylene-aromatic copolyesters and poly(*m*-phenyleneisophthalamide) with NMMO

4.1.1. CPE - NMMO Crystal Solvates

Solubility curves for CPEs and PMPIA in NMMO were constructed (Fig. 1) on the base of visual identification of the temperature corresponding to the transition of polymer blends with NMMO monohydrate (MH) to the fully single-phase state (T_{dis}).

As is seen (curves 1–3, 5), the solubility of the tested polyesters and copolyesters in NMMO MH varies in the following sequence HP-6 > HP-10 >PDTOB. Preparation of PDTOB solutions in NMMO MH with concentrations above 20% requires high dissolution temperatures (above 160°C, where CPEs undergo to degradation. Therefore, a higher melting NMMO hydrates should be used, which allow to dissolve up to 60% PDTOB (curve 4) [8].

Thus, the selection of various hydrate forms of NMMO as dissolving systems for copolymers under study leads us to conclusion, that in both cases: hydrophilic and hydrophobic polymers the dissolving ability of NMMO increases with a decrease in the water content and, accordingly, with increase of the melting point of NMMO.

The DSC data on dissolution of HPs and CPEs in NMMO have shown that the shape of DCS curves for all systems is the same. As an example, Fig. 2 shows the thermograms obtained for the system containing 40% HP-10 in NMMO MH.

As is seen(curve 1), during the first heating the low-temperature hydrate form of NMMO initially melts (the endo effect with a maximum at 36°C) and then the basic melting peak due to NMMO MH (at 76°C) appears. As follows from the DSC curve, processes accompanied by the exo effect proceed just after the melting of NMMO MH. During the second heating run, the profile of the curve changes drastically: only one new endothermic peak appears whose maximum (curve 2) is above the melting point of NMMO MH but below the melting temperature of the crystalline copolyester.

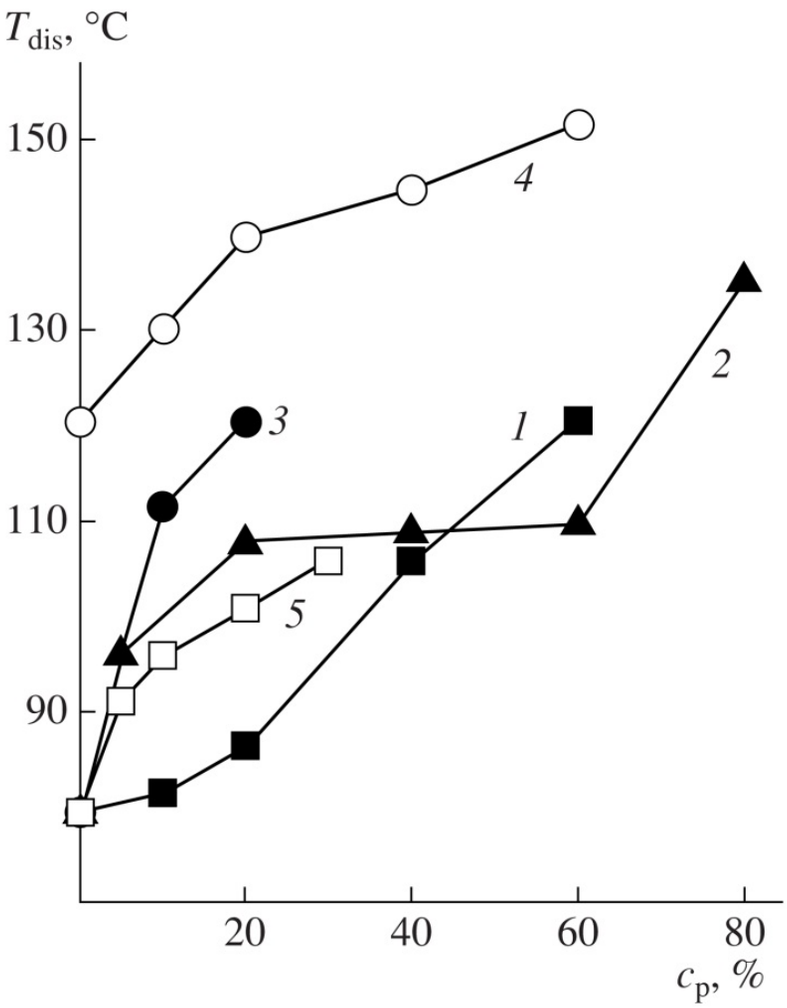

Figure 1. Solubility curves of (1) HP-6 in NMMO MH,(2) HP-10 in NMMO MH, (3) PDTOB in NMMO MH,(4) PDTOB in NMMO, and (5) PMPIA in NMMO MH.

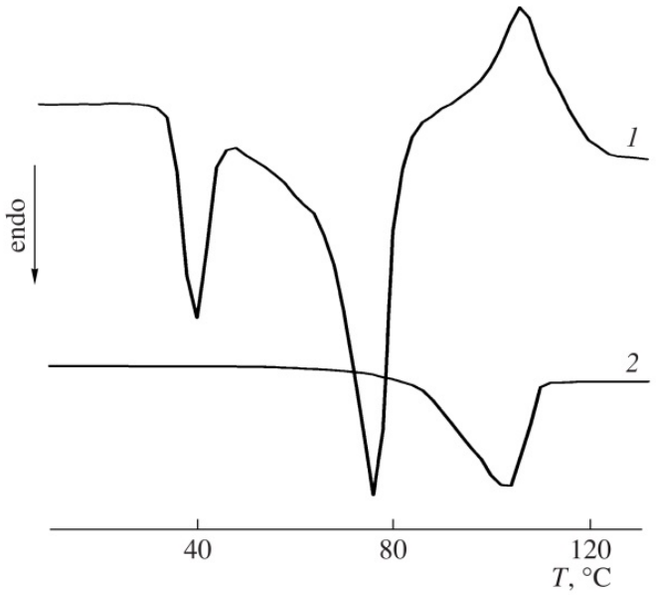

Figure 2. DSC curves of the blend containing 40% HP-10 and 60% NMMO MH under (1) first and (2) second heating runs.

This result allows us to assume that strong interactions between the CPE and solvent molecules exists giving rise to a new additive compound of polymer and solvent having crystalline structure.

Despite of evident information from DSC data concerning the new phase formation in the CPE–NMMO systems (the most probably, crystal solvate, CS), the structure of the novel adduct should be confirmed by X-ray diffraction measurements.

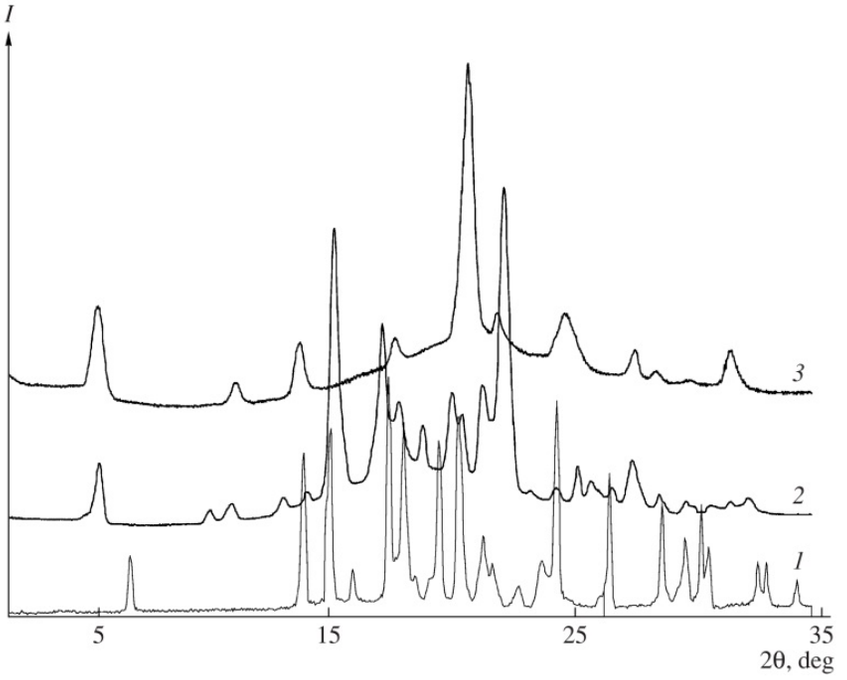

Figure 3. Diffractograms of (1) the NMMO MH solvent, (2) 40% HP-10 solution in NMMO MH, and (3) HP-10 homopolymer at 20°C.

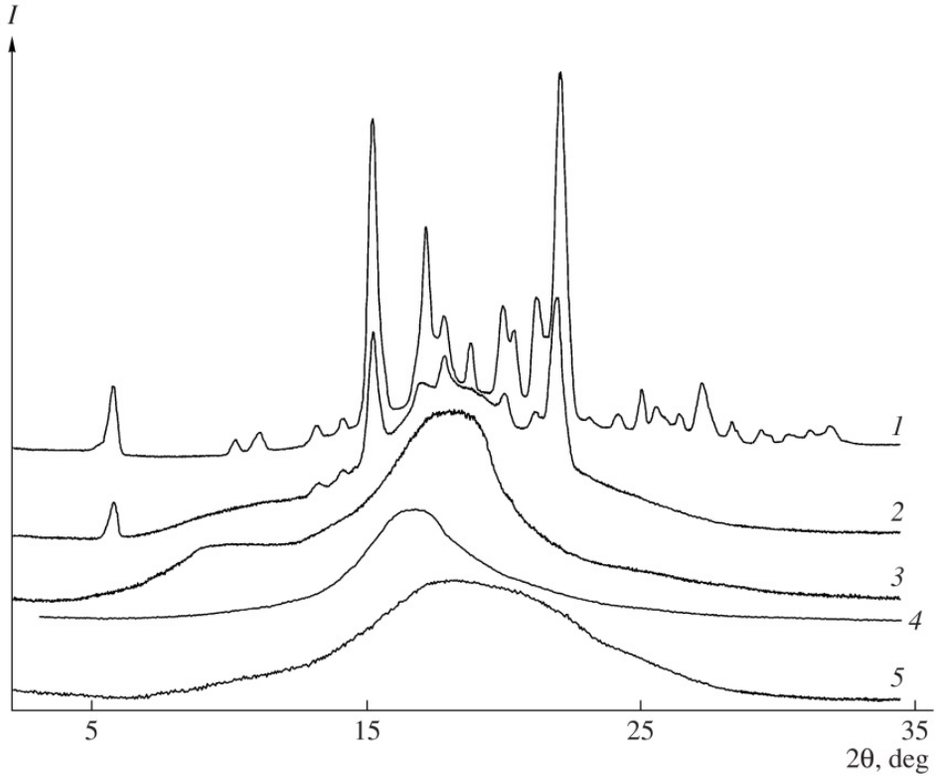

Figure 4. Diffractograms of 40% HP-10 solution in NMMO MH at (1) 20, (2) 110, and (3) 120°C; (4) NMMO MH at 90°C; and (5) HP-10 at 200°C.

Figure 3 displays the diffractograms of the parent compounds — HP-10, NMMO MH, and HP-10 solution in NMMO MH at 20°C. As is seen, the angular positions of $2\theta_i$ reflections measured for the solution differ appreciably from the corresponding $2\theta_i$ values for NMMO MH and HP-10. A specific feature of the diffractograms obtained for the solution and the parent HP-10 samples requires special attention. The first three reflections observed in the diffractogram of the neat HP-10 are manifested in the diffractogram of the solution. The same angular positions of these reflections in the diffractogram of HP-10 and its solution in NMMO MH suggest that NMMO MH molecules are embedded between macromolecules of the polymer causing the change its intermolecular order, at preserving intramolecular periodicity.

This assumption is supported by the X-ray data obtained upon solution heating (Fig. 4). As is seen, the diffractogram of the 40% HP-10 solution measured at 120°C shows three overlapping amorphous halos with maxima at $2\theta = 11.6°$, 18.1°, and 23.5° and the ratio of intensities I1 : I2: I3 = 61 : 100 : 38. Such a pattern of the diffractogram remains unchanged when the sample is heated. This circumstance indicates that the melting of the sample is not accompanied by its decomposition (congruent melting).

In the case of the solution, the center of gravity of the first two amorphous halos is markedly shifted to small angles (larger interplanar distances) compared with the HP-10 melt, for which the intensity curve of amorphous scattering contains a single amorphous halo with a maximum at $2\theta = 19.1°$. Such significant changes in the intensity distribution of amorphous

scattering at passage from HP-10 to its solution in NMMO MH suggest that the statistics of distribution of intermolecular distances changes.

The X-ray pattern of the crystalline adduct of HP- 10 with NMMO MH exhibits a large number of Debye rings with a nonuniform intensity distribution (the presence of discrete spots along rings), thereby indicating a coarse-grained solvate structure with a crystallite size L > 1000 Å. These values of L are untypical for polymer crystals (for the L values, as a rule, do not exceed 400 Å). The X-ray patterns of HP-10, NMMO MH, and the proposed crystal solvate formed by HP-10 in the NMMO MH solution at a concentration of 40% are characterized by completely different crystal lattices. Hence, the structures of the crystalline phase are quite different.

The above experimental data allow us to conclude with a sufficiently high probability that, in the course of CPE dissolution in NMMO MH at elevated temperatures and subsequent cooling of these solutions, new structures—crystal solvates (CSs) of CPEs with NMMO are formed. The phase composition of crystal solvates depends on the polymer-to-solvent molar ratio. The temperature position of the endo peaks in DSC curves due to the melting of CSs changes and achieves a maximum and constant value at the molar ratio of the components that corresponds to the equilibrium composition of the crystal solvate. Thus, the DSC profiles of the systems containing 20–60% HP-10 in NMMO MH are characterized by the presence of constant heat effects at 100–105°C, thus suggesting the equilibrium nature of the crystal solvate phase formed in this concentration range. The formation of CSs of a constant molar composition is also proved by the presence of a plateau in the solubility curve of HP-10 in NMMO MH (Fig. 1, curve 2) at 100–105°C, that is, at a temperature corresponding to T_m of HP-10/ NMMO MH crystal solvates.

These results are in good agreement with X-ray measurements. The diffractograms of systems containing 20–50% HP-10 in NMMO MH are practically identical. Consequently, in the range of HP-10 concentrations in NMMO MH from 20 to 40%, a polymer-to-solvent molar ratio equal to 1 : 5 that corresponds to the equilibrium composition of.

The formed CSs are distinguished by improved stability to water since they preserve their structure when more than 80% water is added to the system. At this content of water, the NMMO multi hydrates occur in the liquid state. Most probably, macromolecules of the hydrophobic polymer protect water-sensitive NMMO molecules; as result, hydrophobic crystal solvates of HP-10 with NMMO MH are formed.

Optical microscopy was applied to analysis of morphological features of CSs. The known morphological kinds of CSs belong to faceted structures (rhombs and parallelograms), spherulites, and shish kebab.

Figure 5 demonstrates micrographs of CSs in crossed polars for the co-crystallization of HP-6, CPE, and HP-10 copolymers with NMMO MH. All crystal solvate structures belong to various types of branched crystals—dendrites. The development of the CSs morphology is a multifactor process influenced by the components nature and crystallization conditions. Thus, the concentration of solution, its prehistory, the time of solution aging at a

temperature above the melting point of the CS, and the rate of cooling affect not only the size of the structures being formed by also the details of their morphology.

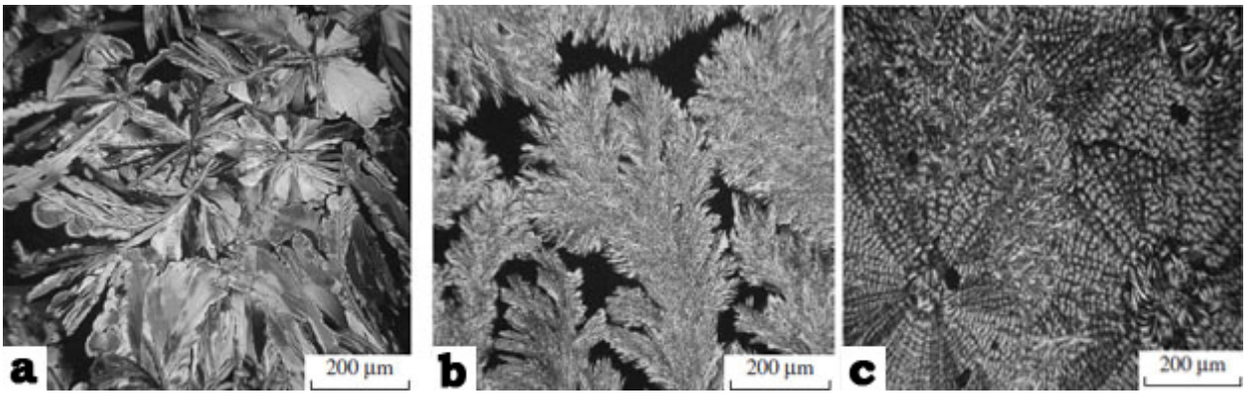

Figure 5. Dendrite structures in systems: (a) 40% HP-6 solution in NMMO MH, (b) 30% CPE solution in NMMO MH, (c) 40% HP-10 solution in NMMO.

4.1.2. PMPIA–NMMO Crystal Solvates

The aromatic polyamide (PMPIA), like the thermotropic alkylene-aromatic CPEs, dissolves rather easy in NMMO MH. As follows from Fig. 1 (curve 6), the resulting solutions contain more than 30% PMPIA. The DSC data for solutions of PMPIA showed that though general tendencies observed for solutions of CPEs in NMMO, namely, formation of additive compounds (CSs) are preserved, the character of structure formation occurring during dissolution of PMPIA in NMMO is more complicated. Thus, the DSC curves measured for solutions containing 5–10% PMPIA in NMMO MH show two exothermic peaks with maxima at 86–94°C along with endothermic peaks corresponding to the melting of NMMO bihydrate (T_m = 36°C) and NMMO MH (T_m =76°C). The appearance of the exothermic peaks indicates on formation of new additive compounds of PMPIA with NMMO MH. (Fig. 6).

The profile of the DSC curves obtained for PMPIA solutions prepared in the high-melting NMMO (T_m = 110–120°C) is identical to that of the DSC curves of PMPIA solutions in NMMO MH and only positions of exothermic peak maxima corresponding to CSs formation are different. For CSs, the values of T_m vary in a wide range from 103 to 135°C.

X-ray analysis of 5–20% PMPIA solutions in NMMO MH and in high-melting NMMO has shown that various types of ordered solvate systems may be formed depending on the hydrate form of the starting NMMO. In Fig. 7, the diffractograms of 5 and 15% PMPIA solutions in NMMO MH as well as individual components at various temperatures are compared. The diffractogram of PMPIA (Fig. 10, curve 6) exhibits two overlapping amorphous halos with maxima at 2θ* ~ 13.9° and 23.3° with the ratio of integral intensities equal to 1 : 5 ($I_1 : I_2 = 1 : 5$). The diffractogram of the individual NMMO MH at 20°C (Fig. 7, curve 1) shows a set of reflections whose angular positions are in agreement with the data from. The scattering picture of the NMMO MH melt (Fig. 7, curve 7) is characterized by the presence of a single amorphous halo at 2θ* ~ 16.9°. In the case of PMPIA solutions in NMMO MH, the scattering pictures turn out to be qualitatively different (Fig. 10, curves 2,

3). These pictures show an amorphous peak at $2\theta_1$ ~ 6.8° along with a certain set of rather well-resolved reflections in $2\theta_2$ region 17°– 30°. When the solutions were heated to 95°C, the amorphous halo observed at $2\theta_1$ was conserved despite of a small shift toward small angles (to 6.5°), while all reflections at $2\theta_2$ are disappeared and the amorphous halo peaking at $2\theta_2$ ~ 16.8° is appeared again.

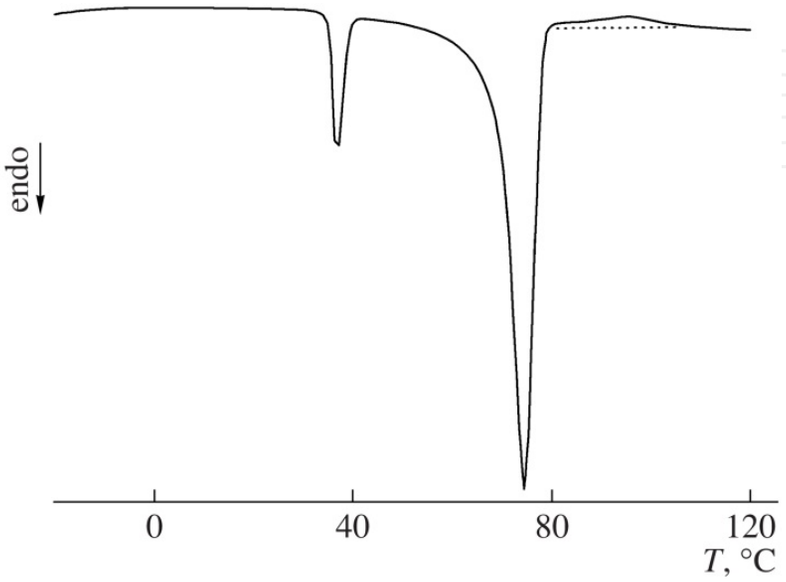

Figure 6. DSC curves of the blend containing 5% PMPIA in NMMO MH.

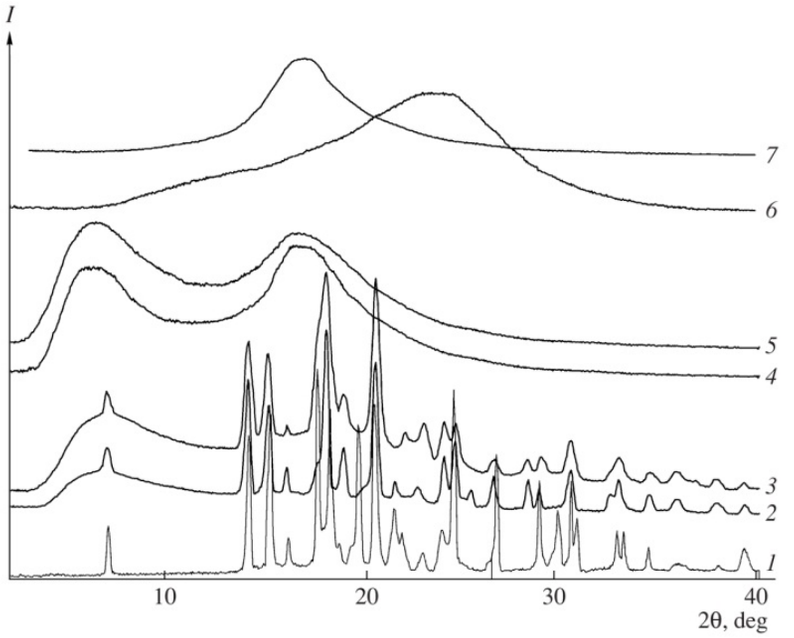

Figure 7. Diffractograms of (1) NMMO MH; (2) 5 and (3) 15% PMPIA solutions in NMMO MH at 20°C; (4) 5 and (5) 15%PMPIA solutions in NMMO MH at 90°C; (6) PMPIA; and (7) NMMO MH melt at 95°C.

A comparison of the intensity distribution of amorphous scattering for the individual PMPIA and NMMO MH and their solution leads us to suggestion that the resulting solutions are not single-phase. The amorphous phase of solutions is predominantly formed

by PMPIA macromolecules solvated via specific interactions with solvent molecules. Another phase of solutions is enriched with solvent molecules and is characterized by scattering at 2θ2 ~ 16.8°. The formation of such phase structures with intermolecular distances d = 13.0–13.6 Å, as calculated from the angular position of the first amorphous halo at $2\theta_1$ was proved by an increase in the ratio of integral intensities of the first and second amorphous halos ($I_1 : I_2$) with increasing content of PMPIA in solution.

The diffractograms of PMPIA solutions in the high melting NMMO display a single amorphous halo in the large-angle region with a maximum at 2θ* ~ 19.1° and a set of discrete Bragg reflections localized against its background. Under heating to 125°C, the melting of the ordered phase takes place, the intensity of the amorphous halo grows, and the angular position of its maximum shifts toward small angles - to 2θ* ~ 17.7°. Note that the 2θ* value for the PMPIA solution at 20 and 125°C differs substantially from the corresponding value for the NMMO melt (2θ* ~ 16.9°). Consideration of this fact coupled with features of the diffractogram measured for the individual PMPIA, such as presence of two overlapping amorphous halos with maxima at 2θ* ~ 13.9° and 23.3° ($I_1 : I_2 = 1 : 5$), results in conclusion that the solution may be considered as single-phase. The melting point of the CS prepared in the high-melting NMMO is much higher (120–123°C). Thus, at a smaller content of water in NMMO, a high-melting crystal solvate phase of PMPIA with NMMO is formed.

The morphology of the crystal solvates formed in the PMPIA–NMMO system are different. Thus, CSs based on NMMO MH are typical spherulitic with superposition of ring textures of amorphous solvate layers (Fig. 8a), while CSs prepared from the high-melting NMMO are dendrite spherulites (Fig. 8b).

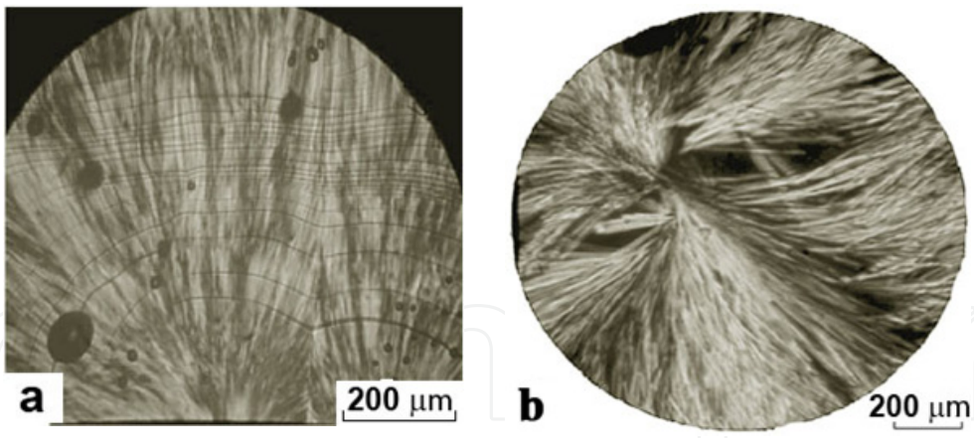

Figure 8. Micrograph of the PMPIA–NMMO crystal solvate prepared in NMMO MH (a) and in the high-melting NMMO (b).

Thus, the experimental evidence showed that the unique properties of NMMO as a high polar donor solvent ensure its high dissolving ability not only with respect to hydrophilic polymers but also with respect to hydrophobic liquid-crystalline CPEs and aromatic polyamides. As a consequence, dissolution processes are accompanied by the formation of CSs of various natures. A high solubility of cellulose and of synthetic polymers under study in NMMO gives us grounds to expect their compatibility in NMMO solutions on molecular level in a certain temperature–concentration range.

4.2. Solutions of Cellulose and its blends with Synthetic Polymers or Layered Aluminosilicates in NMMO

4.2.1. Solutions of Cellulose in NMMO

A highly efficient interaction of NMMO with OH-groups of cellulose is ensured due to presence of a semipolar N —›O bond with two unshared electron pairs at the oxygen atom in the NMMO molecule which can interact with two proton-containing groups. However, despite the high dissolving capacity of NMMO, the preliminary aqueous activation of cellulose is needed to facilitate the access of solvent molecules to the functional groups of cellulose to accelerate dissolution.

The schematic representation of cellulose dissolution in NMMO (diagram in Fig. 9) renders it possible to follow the evolution in the phase composition of the three component cellulose–NMMO–H_2O system during dissolution [5,9-10].

The first stage of the process (swelling of cellulose in aqueous solution of NMMO) proceeds in two stages. The first stage includes the treatment of cellulose with aqueous NMMO solution to produce a homogeneous pulp that contains, as an example, 35% H_2O, 9% cellulose, and 56% NMMO (point C in the diagram). At the second stage, an excess of water is removed to form a homogeneous suspension of the following composition: 20% H_2O, 13% cellulose, and 67% NMMO (point B). After further removal of water excess, dissolution occurs at the following approximate contents of the components: 14% cellulose, 10% H_2O, and 76% NMMO (point A).

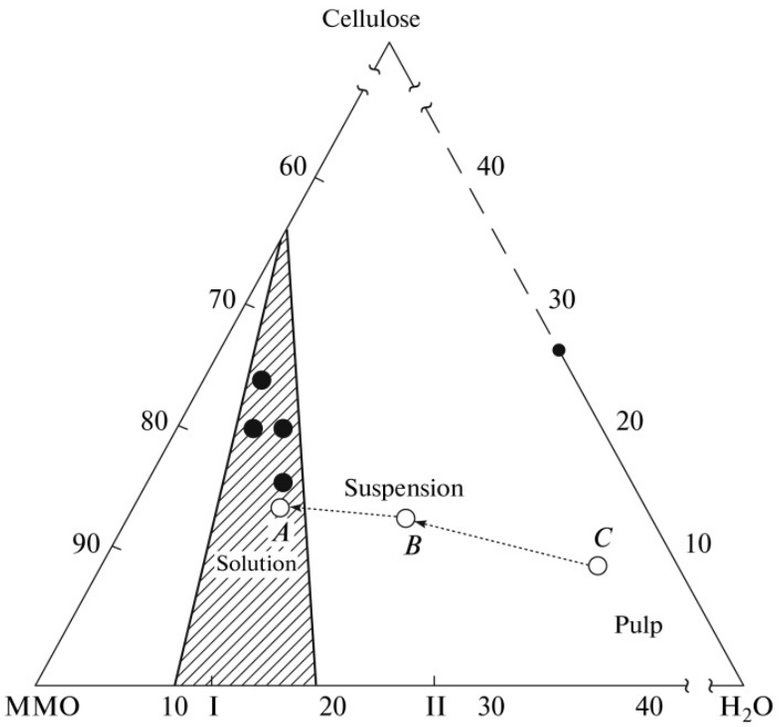

Figure 9. Schematic phase diagram of the cellulose–NMMO–H_2O system: (line CBA) variation in the composition of the system during cellulose dissolution via the traditional NMMO process; (closed circles) composition of the system during cellulose dissolution via the solid phase NMMO process.

A new method of solid-phase dissolution of cellulose in NMMO [6] allows to improve significantly the dissolving ability of NMMO MH using higher activity of high-melting hydrate forms of NMMO. This process involves the stage of solid-phase activation of cellulose by crystalline NMMO, which proceeds under triaxial compression, shearing, and forced plastic flow. Under the conditions of all-hydrostatic compression and shear, the mechanochemical activation of cellulose by crystalline NMMO occurs via formation of H-complexes. At further simultaneous action of temperature and shear rate, solid H-complexes (or solid precursors of solutions of cellulose in NMMO) melt and transform into highly concentrated flow solutions with a high level of homogeneity.

Thus, the solid phase process is distinguished by the invariable phase composition of the system during cellulose dissolution, beginning from the stage of preparing solid presolutions to their melting and transition to the liquid state, as illustrated by the position of corresponding points in the schematic diagram (Fig. 9). Four points shown in the diagram correspond to solutions with different concentrations of cellulose ranging from 16 to 25% prepared via solid-phase activation.

Preparation of cellulose solutions in NMMO in a sufficiently wide concentration range gave us the supplementing information on the phase state of the NMMO–H_2O–cellulose system and completing the phase diagram in the range of cellulose concentrations from 0 to 50% (Fig. 10) [11].

The lines of phase equilibrium are constructed from melting points from DSC curves, X-ray data, and polarizing microscopy data. Highly concentrated solutions of cellulose in NMMO are inclined toward supercooling, and they do not solidify at room temperature after heating for several months. These circumstances make attainment of the equilibrium state extremely difficult.

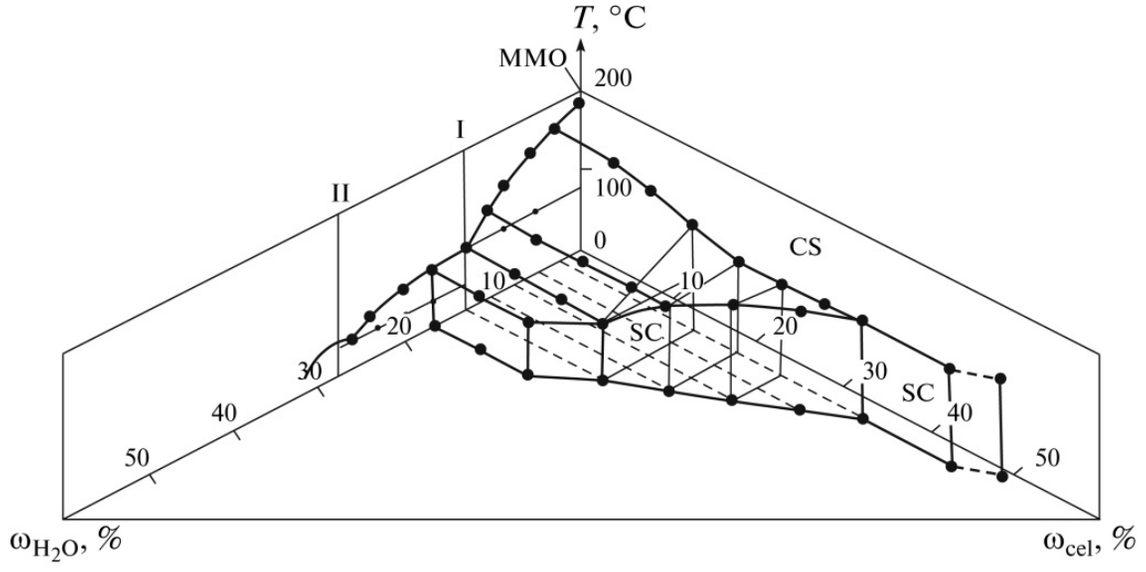

Figure 10. 3D state diagram of the cellulose–NMMO–H_2O system: SC is the solid H-complex, CS is the solution of cellulose in NMMO. (I) NMMO 2.5-hydrate and (II) NMMO monohydrate.

Although the above phase diagram is demonstrates clear conditions for the formation of highly concentrated solid complexes of cellulose with NMMO and the temperature–concentration regions of their transition to the flow state. As is seen from the diagram, the position of liquidus lines reflecting the melting temperatures of solid complexes helps us to choose appropriate variables to obtain dopes of different composition. This tendency becomes more pronounced with an increasing concentration of cellulose in solution.

4.2.2. Phase equilibrium in mixed solutions of cellulose with synthetic polymers in NMMO

As was shown above, the unique properties of NMMO as a highly polar donor solvent are responsible for its high dissolving ability not only for hydrophilic but also for hydrophobic polymers. Numerous studies have been devoted to the problem of solubility of polymers in ternary systems composed of two polymers and one solvent. The number of polymer pairs that can be dissolved in one common solvent is very limited, and all polymer solutions tend to undergo phase separation even at low concentrations [12]. Therefore, complete compatibility of polymers, which is primarily controlled by the nature of a solvent, is the exception rather than the rule.

The phase state of ternary HP(CPE)–cellulose–NMMO systems was studied by polarizing microscopy, turbidimetry, visual observations, and rheological studies over a wide range of concentrations of polyesters and cellulose when the overall content of polymers was 35%. All solutions are optically isotropic and do not show any birefringence.

To estimate the limiting compatibility of cellulose and polyesters in common solvent, phase state diagrams are constructed for two systems: cellulose–CPE–NMMO and cellulose–PDTOB–NMMO [13]. Taking into account all experimental implications in the construction of 3D phase state diagrams, we studied the phase equilibrium on the cross section of the 3D diagram at a constant temperature of 120°C.

Figure 11 presents the fragment of this cross section. The upper point of the triangle corresponds to 100% NMMO, whereas the left-hand and right-hand corners correspond to 100% of cellulose and 100% of CPE, respectively. The binodal is the boundary line describing amorphous equilibrium. Under binodal the transition of the cellulose–CPE–NMMO system from the single-phase to the two-phase state takes place. Above the binodal, the system is thermodynamically compatible and has below the binodal, the system undergoes phase separation.

As was shown in [24], among all CPEs under study, PDTOB has the lowest solubility in NMMO; however, according to the phase diagram, the cellulose–PDTOB–NMMO system (binodal 2) is characterized by a higher level of compatibility between components than the cellulose–CPE–NMMO system (binodal 1). Since CPE has higher solubility in NMMO, one could expect that the corresponding phase equilibrium curve in ternary system should be located under the bimodal 2; however, contrary to expectations, the binodal 1 appears to shift towards lower concentrations of polymers.

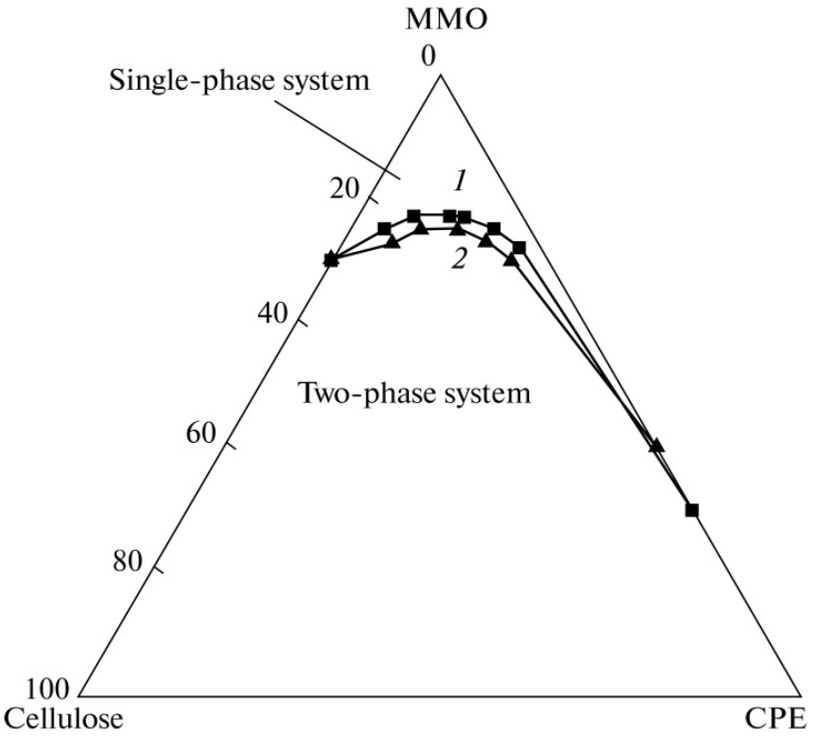

Figure 11. Phase state diagram for ternary systems at 120°C: (1) cellulose–CPE–NMMO and (2) cellulose–PDTOB– NMMO

The heterogeneous character of the single-phase mixed solutions of cellulose and CPE was studied by spectroturbidimetry (Fig. 12).

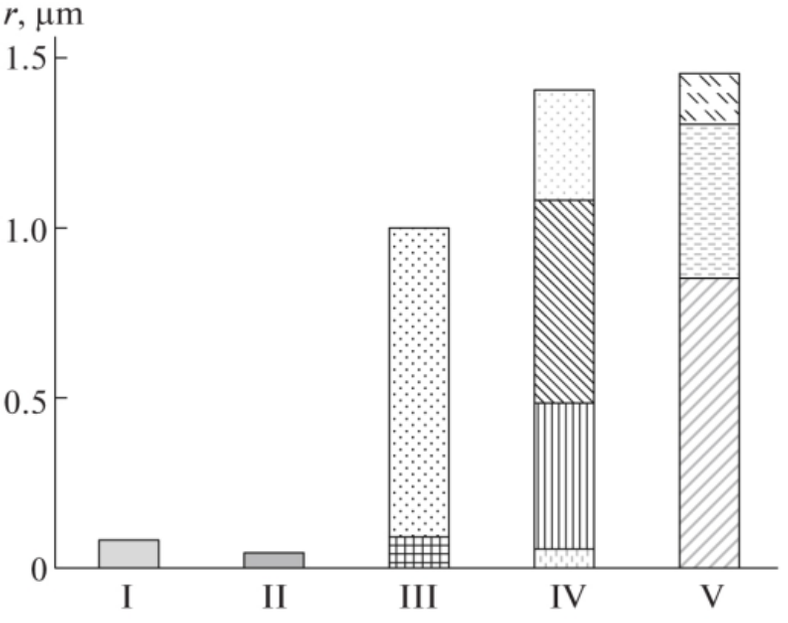

Figure 12. Histogram of heterogeneity in the cellulose–CPE–NMMO system: (I) 10% cellulose solution in NMMO; (II) 15% solution of CPE in NMMO, and (III–V) mixed cellulose–CPE solutions in NMMO: (III) 10 : 5, (IV) 10 : 10, and (V) 10 : 15%.

As compared with solutions of neat components, the measurements have demonstrated a significant increase in heterogeneity of the mixed solutions. Upon the addition of CPE, for example, to cellulose solution one can reasonably suggest that due to higher rate of dissolution in NMMO this component quickly transforms into solution and cellulose now became dissolved not in pure NMMO but in its polymer-containing solution. Since the thermodynamic quality of the "dissolving system" with respect to cellulose is reduced, the interaction between cellulose macromolecules increases, leading to formations agglomerates and aggregates that causes increasing the heterogeneity of the mixed solution. As the concentration of CPE is further increased (the region below the binodal), the system undergoes amorphous separation and the two-phase emulsion is formed. At higher concentrations of CPE, the dissolving potency of NMMO with respect to cellulose dramatically decreases and fraction of undissolved cellulose appears in a system.

In contrast to the mixed solutions of cellulose and CPE in NMMO, which are single-phase systems over a wide concentration interval up to an overall content of polymers in solution of ~20%, all mixed solutions of cellulose and PMPIA in NMMO are biphasic. Thermodynamic incompatibility of solutions results in development of fascinating morphological effects in two-phase solutions of PMPIA–cellulose mixtures in NMMO. Optical observations showed that cellulose solutions in NMMO containing 1–5% of PMPIA are emulsions. The droplets of the dispersed phase are nearly spherically shaped, and their size distribution is rather wide (Fig. 13a). All droplets are exceptionally labile and already at weak shear deformation, break down into smaller-sized droplets, which can be extended and form threadlike fibrous structures (Fig. 13b). As a result, highly regular fibrillar morphology with high periodicity in the arrangement of fibrils in the bulk phase is formed.

This phenomenon is most pronounced upon the extrusion of mixed solutions through a capillary rheometer. The entrant region, where convergent flow and stretching takes place, provides more favorable conditions for the development of fibrillar morphology. The use of detachable capillaries allowed us to study flow morphology by visualizing the evolution of optical patterns of the samples collected from a capillary and from various regions of the inner chamber of micro viscometer. The collected samples were studied using a polarizing microscope. As was found, in the mixed cellulose–PMPIA–NMMO systems, the formation of fibrils was observed even in the chamber of the viscometer at a distance of ~10 mm from the entrance to the capillary channel (Fig. 13c). Fibrils achieve their maximum level of regularity in the capillary (Fig. 13d) and, especially, upon drawing of extrudate in the exit zone (Fig. 13e). Under the action of extension and shear stresses, the dispersed phase formed by flexible-chain PMPIA structures divides (disintegrates) the cellulose solution matrix. Shear stresses induced on interfaces between two incompatible solutions lead to the orientation of the forming macrofibrils. As a result, of the above phase morphological transformations in the mixed cellulose–PMPIA–NMMO systems, especially at a low PMPIA content, a highly ordered fibrillar morphology forms, which breaks down under the action of temperature. For example, when mixed solutions containing 5% of PMPIA are heated at temperatures above 160°C, liquid threads begin to break down and form a necklace of droplets. When in the mixed cellulose–PMPIA–NMMO system, polyamide is the

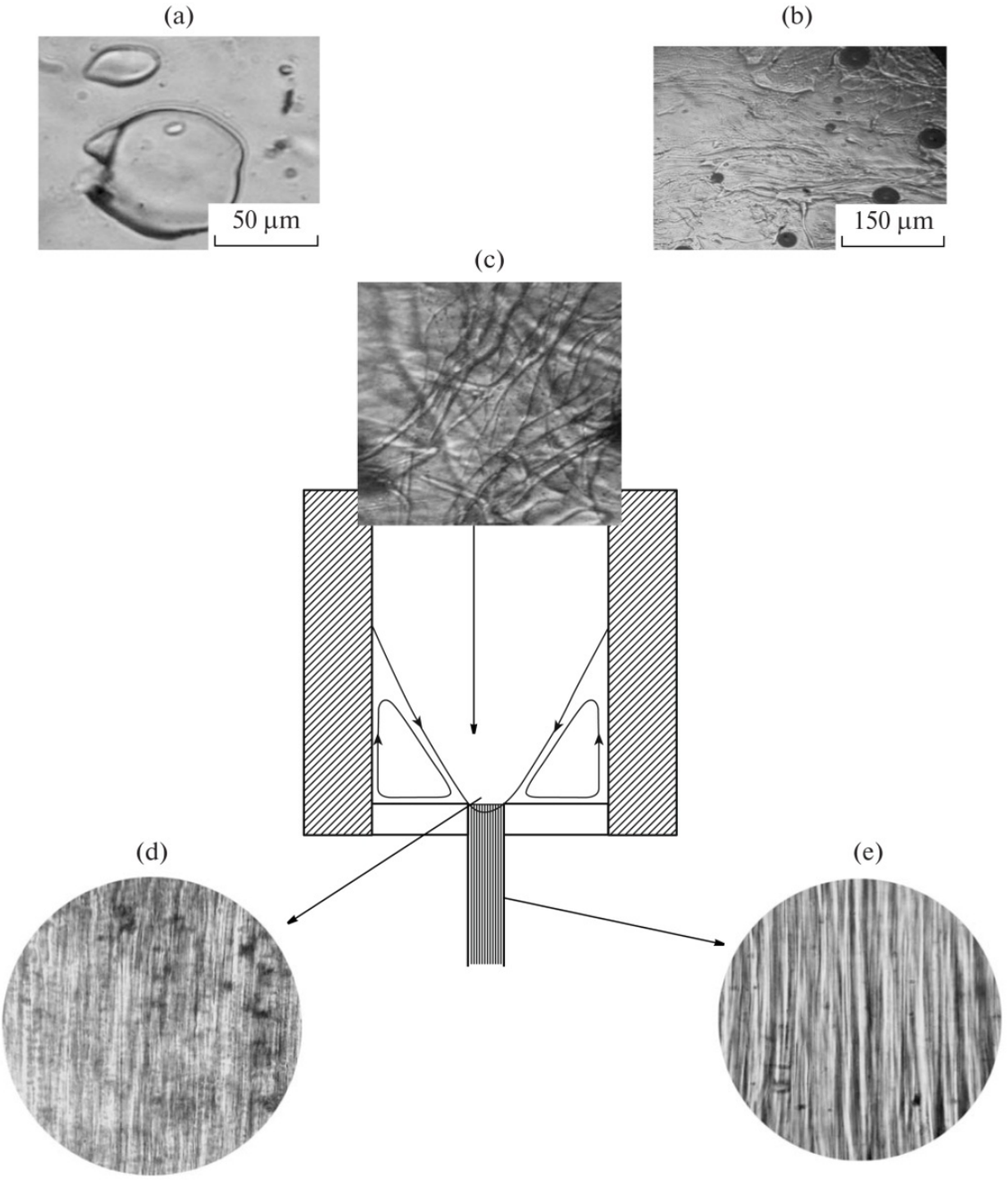

Figure 13. Micrographs of the mixed cellulose–PMPIA solution in NMMO with a concentration of 18% and with a ratio between components of 17 : 1: (a) the test sample is sandwiched between glasses on a hot table of polarizing microscope, (b) the same sample under deformation, and (c–e) specimens collected from different regions of capillary viscometer.

predominant component, the fibrillar structure becomes less ordered and more movable. Upon heating, the threads completely degrade already at temperatures below 120°C. As further increase of temperature, the above droplets undergo coalesce.

The homogeneity of cellulose mixed solutions with polyesters in NMMO and the heterogeneity of solutions with PMFIA results in a significant difference in their rheological properties.

4.2.3. Rheological characteristics of mixed solutions of cellulose and synthetic polymers in NMMO

Comparative analysis of viscous characteristics of CPE–cellulose solutions in NMMO let us to conclusion, that the introduction of CPE into cellulose solutions does not change drastically profiles of flow curves or the concentration dependences of the viscosity inherent for binary solutions cellulose-NMMO. At low and intermediate shear rates, mixed solutions demonstrate Newtonian character of flow; at high shear rates, a marked viscosity anomaly is observed. The introduction of CPE into cellulose solutions increases their viscosity in whole range of shear rates. The concentration dependences of the viscosity of cellulose solutions show positive deviations from values corresponding to the logarithmic additivity rule. This indicates on strong intermolecular interactions between molecules of solvent and cellulose as well as between cellulose macromolecules themselves. The introduction of CPE macromolecules into the cellulose–NMMO system gives rise to even higher positive deviations of the concentration dependence of viscosity.

Due to the specific structural features of cellulose and even despite its strong electron donor–acceptor interaction with NMMO, cellulose solutions in NMMO are known to be highly structured. Due to presence of CPE in NMMO, solvent quality decreases and interaction between cellulose macromolecules appears to be enhanced; as a result, the viscosity of the mixed solutions is increased. Therefore, the difference between binary and ternary solutions is concerned with the level of structural organization of cellulose macromolecules.

Hypothetically, the high level of structuring of the mixed solutions increases with increasing overall concentration of polymers and variation in the ratio between components. As a result, mixed solutions are metastable. This assumption was proven by rheological studies performed for mixed solutions cellulose and CPE in NMMO over a wide concentration interval.

For example, at passing to 25% mixed solution concentration, which according to ternary phase diagram is located in vicinity of the binodal, the character of rheological behavior changes, especially in the regions of limiting concentrations (20% of cellulose/5% of PDTOB and 5% of cellulose/20% of PDTOB). For example, in the case of the 20/5 mixture viscosity anomaly at high shear stresses increases dramatically. Flow curves of the 5/20 mixture can change their position depending on prehistory of the sample and deformation conditions. Therefore, deformation of the solutions in their pre-transition region increases phase instability and can lead even to the phase separation. One can expect that for the mixed systems located directly on binodal, the effect of deformation will be the most pronounced.

Figure 14 presents two flow curves for the cellulose-PDTOB (13/15) mixture. Curve 1 corresponds to short deformation times (strain is 10–100 rel. units), and in these conditions the system does not undergo phase separation. With increasing time of deformation action (strain is above 100 rel. units) the shear stress does not grow monotonically at each shear rate, but after reaching the definite strain decreases (stepwise curve). This kind of behavior

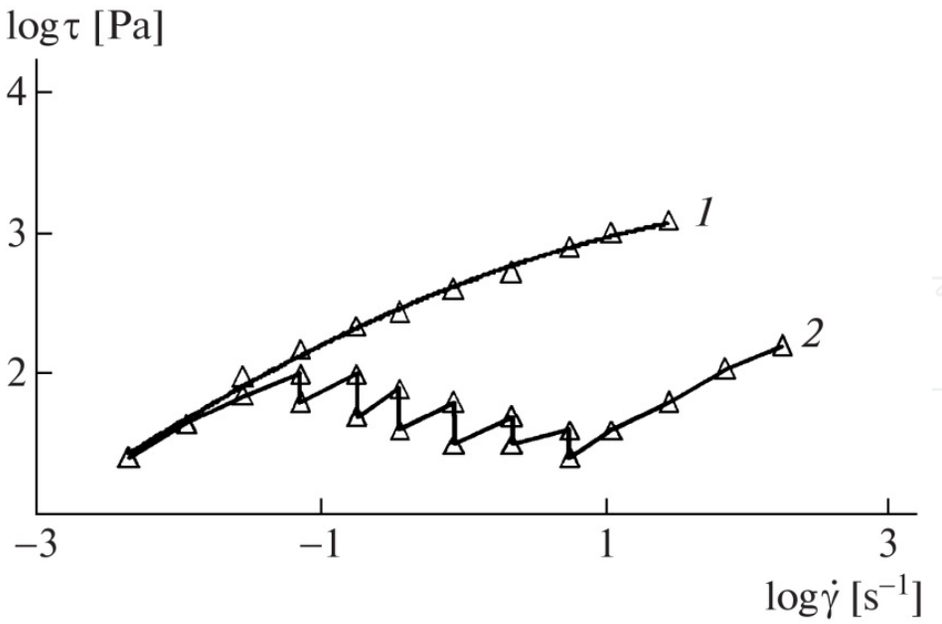

Figure 14. Flow curves of the mixed cellulose–PDTOB solutions in NMMO; overall concentration of polymers is 28%, and cellulose : PDTOB ratio = 13 : 15: (1) small strains, (2) high strains.

reflects transition through binodal induced by strain. By other words, after relaxation at stopping the previous shear rate, the system is homophase but deformation at flow acts as thermodynamic factor changing the bimodal location, and the system becomes heterophasic. Cessation of flow at each shear rate leads to stress relaxation and reverse transition into one-phase region, but new loading causes the same transformation of the phase state. These results indicate on two circumstances: significant changes in the rheological behavior of mixed solutions on passing from the single-phase to the two-phase state, and influence of flow on location of the binodal curve.

Mixed cellulose–CPE solutions in NMMO with phase compositions corresponding to single phase region have been studied over a wide range of shear stresses with attempt to see morphological changes, they have not been revealed.

In contrast to the above systems, two-phase cellulose–PMPIA systems in NMMO are characterized by a well-pronounced heterogeneous morphology, which is controlled by the composition of the sample and deformation conditions. First, let us consider the specific features of the rheological behavior of mixed cellulose–PMPIA–NMMO systems under capillary flow. All solutions that contain 14, 18, and 20% of polymers show a non-Newtonian behavior or, in other words, their viscosity almost linearly decreases with increasing shear stress and follows the power-law flow regime.

The concentration dependences of the viscosity (log τ = 3.6 Pa) were constructed for equi-concentrated mixed solutions; the overall concentration of polymers in solutions was 14 or 18%. As follows from Fig.15, the viscosity of all the solutions lies below the line of logarithmic additivity.

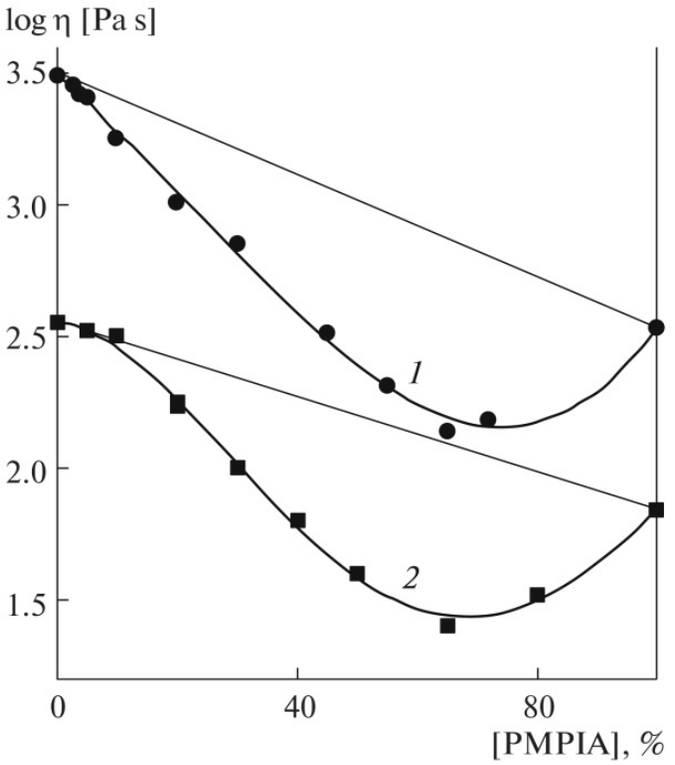

Figure 15. Concentration dependences of viscosity of the mixed cellulose–PMPIA solutions in NMMO. The overall concentration of polymers is (1) 14 and (2) 18%.

On passing through the entrance zone, droplets of PMPIA solution (the dispersed phase) are elongated and transformed into long liquid threads oriented along the flow direction, forming a fibrillar system. As a result, inside the capillary a complex profile of linear velocities is realized (a multi-parabolic one). Due to the superposition of multiple profiles, the overall flow rate decreases.

In addition to capillary viscometry, the rheological behavior of the mixed cellulose–PMPIA solutions in NMMO was studied on a rotation rheometer with its cone–plate working unit. Measurements were performed under steady-state shear by measuring dependences of tangential (τ) and normal (N_1) stresses on the shear rate and in the low-amplitude oscillatory deformation regime by measuring the frequency dependences of storage modulus G' and loss modulus G''. In the case of the first difference of normal stresses, their coefficient connecting N_1 with shear rate was calculated: $N_1 = \zeta \dot{\gamma}^2$.

Figure 16 presents the concentration dependences of the effective viscosity η and the coefficient of normal stresses. As follows from this figure, in contrast to the concentration dependences of viscosity constructed from data of capillary flow, the above mentioned dependences have S-shaped profiles with positive deviation at low concentrations and negative deviation at high concentrations. A slight positive deviation from additivity can be explained by different flow kinematics in rotation and capillary regimes leading to different orientation of the disperse phase droplets.

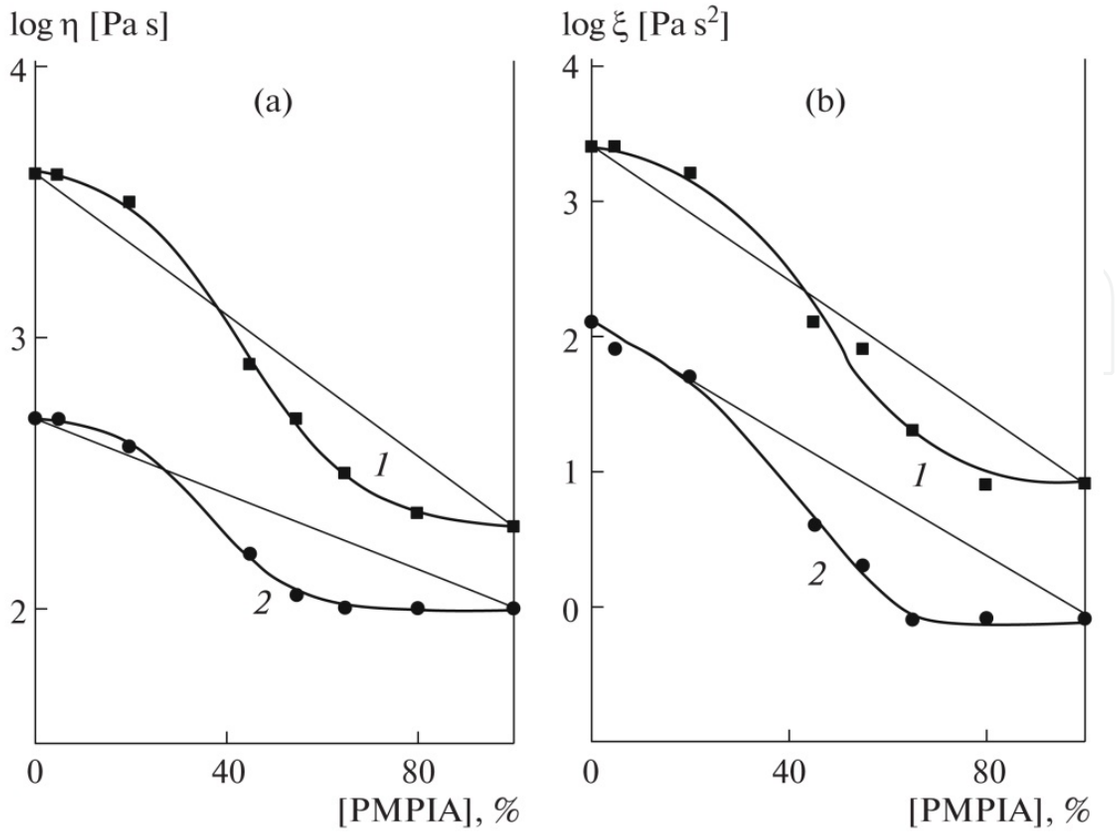

Figure 16. (a) Viscosity η and (b) coefficient of normal stresses ζ vs. composition for the mixed cellulose–PMPIA solutions in NMMO at log τ = (1) 3 and (2) 4 Pa. The overall concentration of polymers is 18%.

The use of the transparent cell as the working unit in the rotation rheometer allowed us to perform the direct visual observation of the behavior of mixed systems under flow. Upon deformation in an uniform shear field, mixed solutions containing from 5 to 40% of PMPIA are transformed into a microheterogeneous system with a highly developed interfacial surface. In the case of 5% content of PMPIA solution, the shear deformation is insufficient to provide any deformation of droplets and they play a role of filler. When the content of the PMPIA phase is increased, the dimensions of droplets increase and the deformation induce the transformation of the droplet-matrix morphology into the fibrillar one. The formation of liquid continuous threads of the dispersed low-viscous phase is accompanied by negative deviations of the concentration dependences of the viscosity from the additive straight line, similar to the case of the capillary flow.

The concentration dependences of G' and G'' as well as steady-state viscosity are S-shaped. According to the traditional concept on the character of flow of incompatible polymer systems, the transition the positive to the negative deviations of viscosity from the additivity line is treated as phase inversion. In our case, the revealed dependences are controlled by changes in the morphology of the flowing mixed system and by its ability for orientation at different by intensity deformation actions.

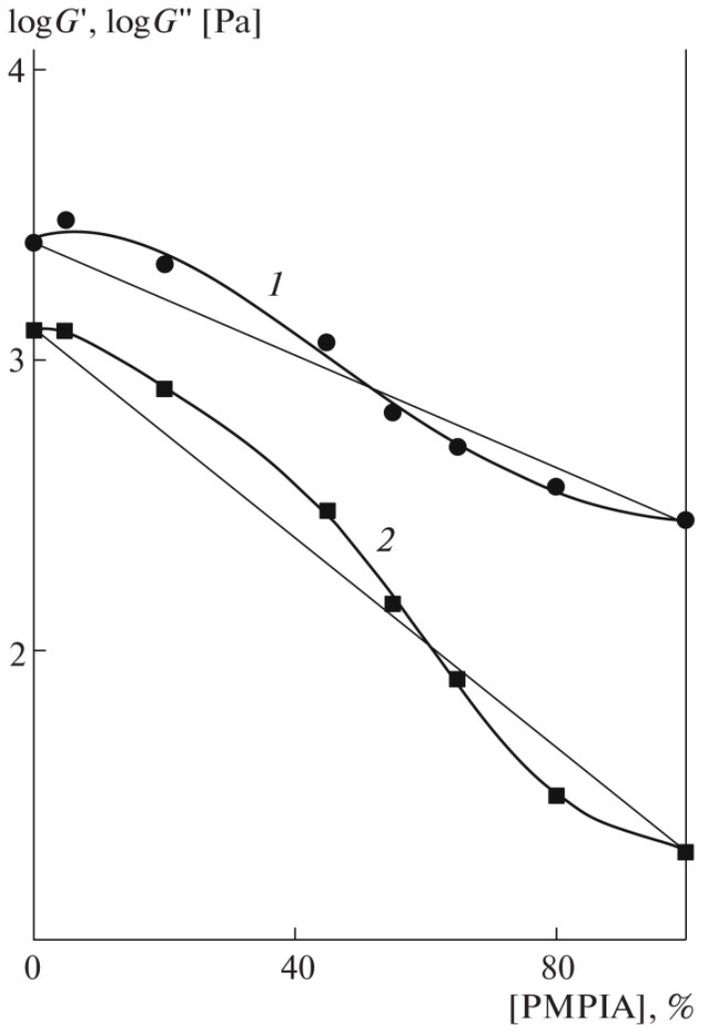

Figure 17. (1) Storage G' and (2) loss moduli G'' vs. composition at $\omega = 1\ s^{-1}$ for the mixed cellulose–PMPIA solutions in NMMO. The overall concentration of polymers is 18%.

Scales of positive and negative deviations can be selected as criteria of the deformability of PMPIA droplets. Depending on droplets deformability at different flow regimes, the interval of inflection shifts along the concentration axis. Maximum positive deviation is for the oscillatory regime. In this case, the point corresponding to the transition to negative deviations is observed at 50–60% PMPIA content. In a homogeneous shear field (under steady-state flow), positive deviations of viscosity are much lower and take place in the concentration interval below 30–40%. Finally, under capillary flow, no positive deviations are observed and maximal viscosity is achieved at ~65% of PMPIA.

Hence, solutions of cellulose and LC copolyesters in NMMO far from binodal change their rheological characteristics according to the traditional mechanism of flow of mixed systems with high specific interaction between components. However, in vicinity of bimodal deformation induces phase transition from the homogeneous to the heterogeneous system leading to unstable flow with oscillation of shear stress. In the case of the mixed cellulose–PMPIA–NMMO systems, the rheological behavior is controlled by transformations of morphology dependent on solution composition and flow regime.

4.2.4. Rheological Characteristics of Mixed Solutions of Cellulose with Natural and Modified Clays

In order to estimate the effect of aluminosilicate additives on the rheological behavior of cellulose solutions in NMMO, rheological properties of filled solutions containing 18 and 10% cellulose were chosen as matrices [14-15]. It was shown that flow of sufficiently viscous 18% cellulose solutions filled up to 9% with different clays is determined mainly by rheological behavior of the polymer matrix. Using less concentrated 10% cellulose solutions allowed to increase the clay content in the solutions up to 20%. The flow curves for 10% cellulose solutions filled to various degree with particles of Cloisite Na^+ are presented in Fig. 18. As is seen from the figure, already at a low content of solid phase the flow of the filled composition becomes a non-Newtonian.

With increasing clay concentration the degree of the viscosity anomaly increases, and at 20% content of clay in the system the shape of flow curve indicates on existence of the yield stress (viscoplastic behavior) due to the formation by filler particles the percolation network. At high shear rates the structure of clay is destroyed, and as a result the rheological behavior becomes similar (pseudoplastic behavior) to cellulose solution in NMMO.

Introducing to the 10% cellulose solution hydrophobic clay - Cloisite 20A is caused some intrinsic features of rheological behavior. The identified features of the rheological behavior of these compositions are presented in Fig. 19 as the generalized concentration dependence of the relative viscosity for both 18% and 10% of matrices containing hydrophilic Cloisite Na^+ and organoclay Cloisite 20A.

For easier comparison, the function is the relative viscosity ($\eta_r=\eta/\eta_{cel}$) , and the argument is a fraction of clay in composition. At the solid content up to 9%, changes of relative viscosity with concentration for all compositions can be described by a single curve, irrespectively of the clay nature and the matrix viscosity. With further increasing of the solid phase concentration the dependence becomes more complex. The single the viscosity-composition curve for solutions filled with Cloisite Na^+ particles does not change, but introduction to solution particles of Cloisite 20A clay leads to a splitting of the curve into two branches. A high viscous branch (curve 1) practically coincident with the concentration curve of systems with natural clay, a low viscous branch lies much lower (curve 2), that is why the generalized dependence for these compositions has a minimum localized at 10% of clay in solution. Starting with concentration corresponding to the splitting, the flow curves of filled solutions containing 15% - 20% of Cloisite 20A demonstrate the presence of the yield stress.

Unexpected at first sight the experimental fact of reduction of the viscosity of filled solutions with Cloisite 20A (curve 2) seems to be explained by different prehistory of their preparation. Within variety of many factors that determine the specific features of systems under investigation, as the main parameter the moisture content in “initially hydrophobic” clay was chosen, since all other components are hydrophilic containing almost equilibrium moisture, meanwhile the sorption of water by hydrophobic clay was unknown.

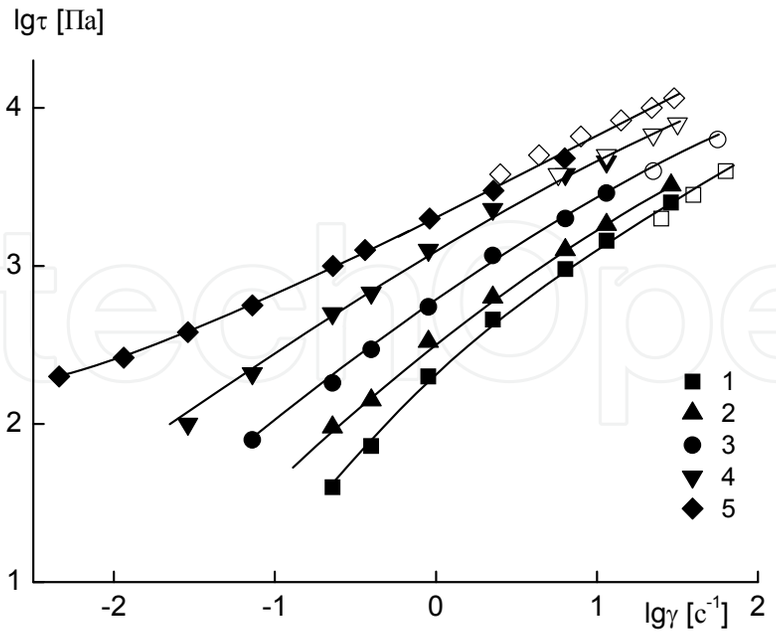

Figure 18. Flow curves for 10% solutions of cellulose in NMMO with Cloisite Na^+. Content of clay: 0 (1), 5 (2), 10 (3), 15 (4), 20 wt.% (5). Filled points - rotational viscometry data, open points - data of capillary viscometry.

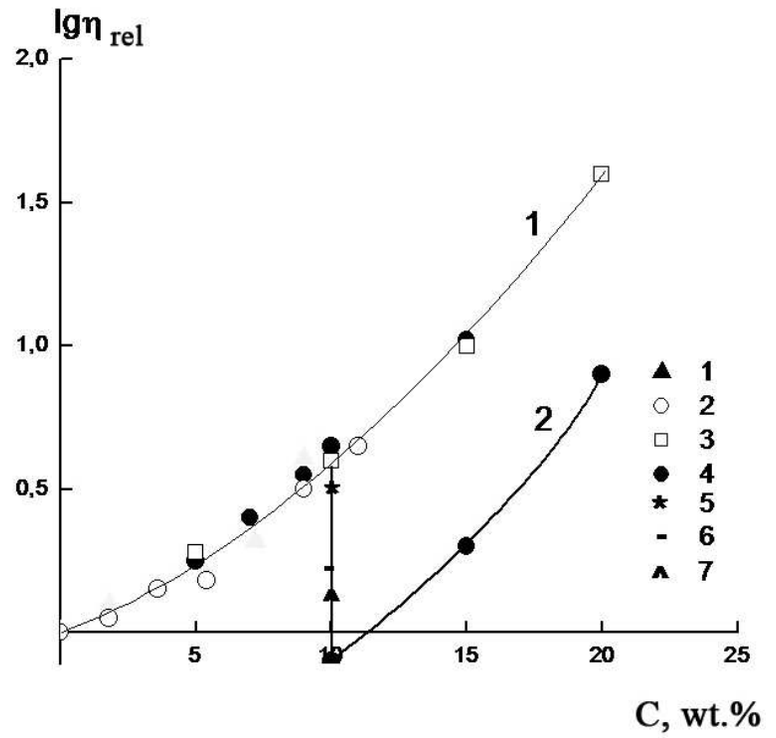

Figure 19. Concentration dependence of the relative viscosity filled solutions of cellulose in NMMO with Cloisite Na^+ and Cloisite 20A at log τ = 3.0 [Pa]. 1-18% solution of cellulose + Cloisite Na^+; 2 - 18% solution of cellulose + Cloisite 20A, 3 - 10% solution of cellulose + Cloisite Na^+; 4 -10% solution of cellulose + Cloisite 20A. Figures 5, 6 and 7 correspond to 6, 13 and 16% of moisture content in Cloisite 20A.

Model experiments on influence of moisture content in Cloisite 20A on the viscosity values using pre-moistened clay with a fixed water content were carried out. Obtained results have confirmed the assumption that a decrease in the viscosity of filled solution is caused by increase of water content in the clay. By means of X-ray diffraction method, a comparative structure analysis of the neat clay (~ 2% of water) and extremely Cloisite 20A moistened after prolonged sorption up to 16% of water it was shown that the basal reflection of neat clay at 2θ, equal to 3,2° transforms to diffuse asymmetric reflection with maxima at 2θ 2,6° and 3.9° for moistened clay (Fig. 20). Such change of the diffraction pattern indicates on specific ability of clay hydrophobized with quarterly ammonium bases to absorb water. We can expect that water molecules should come to the polar Na^+ center of ionic surfactant localized on negative clay platelets. On the one side, this can lead to increase of the interplanar spaces, i.e., to decrease of the intrinsic scattering angle, but on the other side, presence of polar water molecules in vicinity of hydrophilic clay elementary platelets could cause hydrophobic interaction (repulsion) that change conformations of hydrophobic tails of modifier leading to their shrinking. As a result of dual action of water molecules, the interspace width change in non-homogeneous manner (extension-shrinkage).

Rheological data show that 10% content of clay in the system is critical, at which heterophase structure of the interplanar spaces forms and can initiate distortion of clay crystalline structure with formation of irregular layers. Shear action can cause fragmentation of clay platelets ensembles accompanied by a drop in the viscosity of the system as whole.

Introduction to the cellulose solutions of nanoparticles of M_2Cloisite Na^+ in amount not exceeding 0.1% leads to decrease of the solutions viscosity more than in two times (Fig. 21).

Filled solutions of cellulose in NMMO with addition of nanoparticles of M_2Cloisite Na^+ are characterized by a pronounced fibrillation. Apparently, the reason of reducing the viscosity is directly related to the fibrillar structure of cellulose solutions in presence of clay nanoparticles and extremely high surface energy of highly developed interfaces.

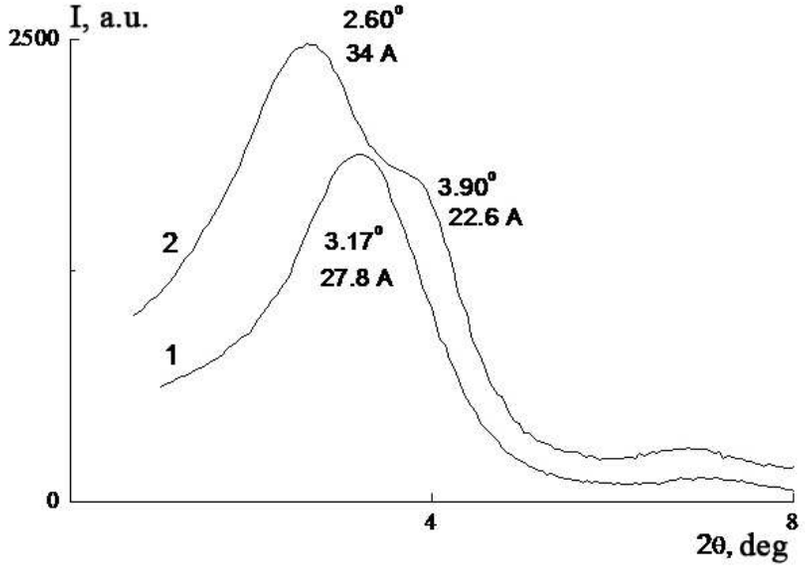

Figure 20. Diffraction patterns of the neat Cloisite 20A (1) and moistened Cloisite 20A (2).

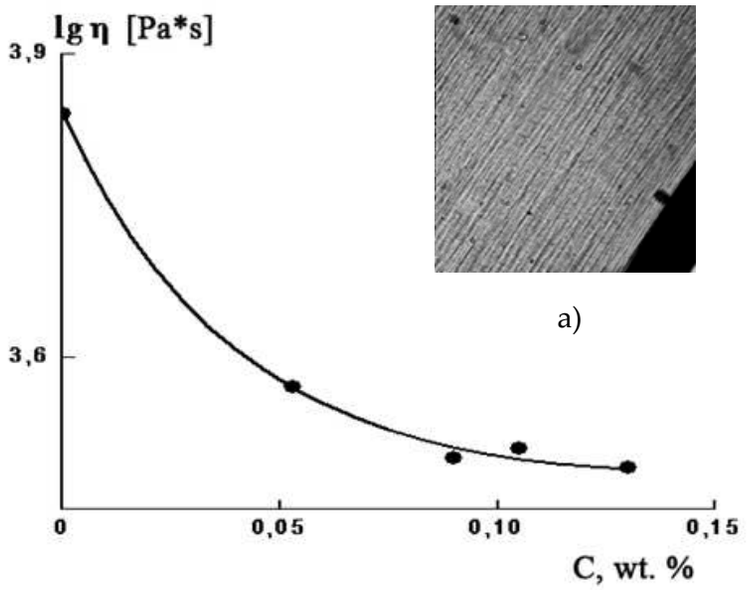

Figure 21. Dependence of the viscosity on concentration of M_2Cloisite Na^+; a) Microphotography of 18% cellulose solution with 0,03% M_2Cloisite Na^+.

The rheological behavior of filled solutions of cellulose with microparticles of Cloisite Na^+ and Cloisite 20A is similar to the behavior of traditional polymer filled systems, while in presence of nanoparticles the flow mechanism changes from traditional segmental to stratified one, i.e., stream morphology becomes regular.

5. Evolution of cellulose structure at transition from dopes to cellulose and blend oriented fibers

5.1. Structure of cellulose and its blends with synthetic polymers

X-ray data demonstrate that solutions containing 18% cellulose in NMMO are amorphous and isotropic, as evidenced by the short-range order in the arrangement of macromolecules. The bulk extrudate obtained without drawing after full removal of the solvent is likewise isotropic, as is seen from X-ray patterns shown in Fig. 22a.

Spinning of fibers from 18% cellulose solution leads to substantial changes in the cellulose structure. The as-spun fiber containing the residual solvent is characterized by nonequilibrium metastable modification of cellulose. The X-ray pattern of this sample (Fig.21b) exhibits well-defined equatorial reflections. Presence of only one intense reflection on the equator of the diffractogram implies that the intensity abruptly declines with the diffraction angle 2θ. This effect is usually attributed to an increase in the disorder owing to the formation of disruptions along chains. A similar character of diffractograms, as a rule, is typical for 2*D* columnar mesophases. During complete phase separation, a crystalline phase of the cellulose is formed (Fig. 22c).

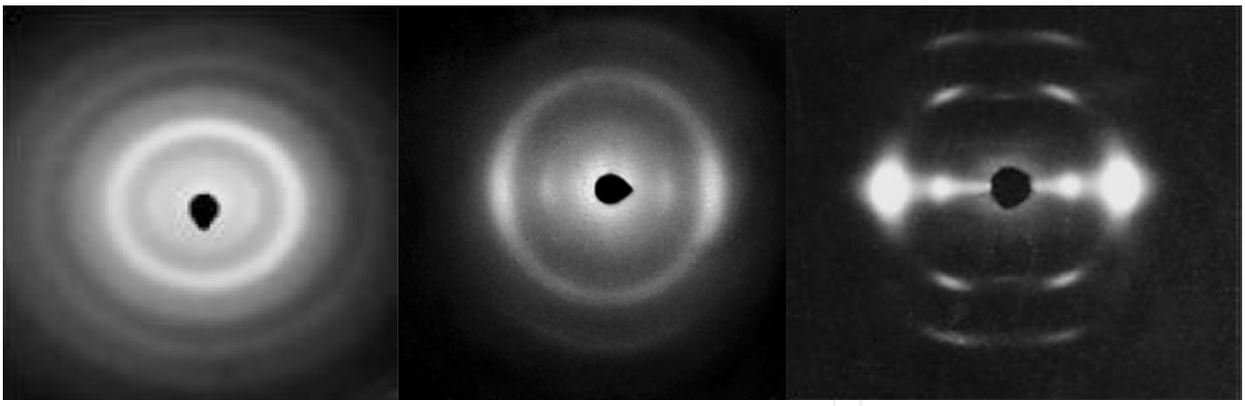

(a) (b) (c)

Figure 22. Flat camera X-ray patterns of 18% solution of cellulose in NMMO (a), cellulose partially washed-out from NMMO (b) and completely coagulated oriented cellulose fibers (c).

During spinning of the cellulose fiber from NMMO solutions, there appears a crystalline phase in which long crystallites are extended in the longitudinal direction [16-18]. On the one hand, this situation indicates on high order and increased density of the structure being formed. On the other hand, this leads to decrease of the probability of transverse hydrogen bonds with neighboring crystalline clusters formation enhancing the tendency of the system toward fibrillation. The transformation of structure in the cellulose–NMMO system during the spinning of model fibers is schematically shown in Fig. 23.

A comparison of X-ray pattern taken for the crystalline fiber (Fig. 22c) and the gel fiber (Fig.22b) of cellulose leads us to suggestion that the package of macromolecules in the plane of the 2D mesophase and the ac plane of the crystal are similar. This conclusion is supported by the fact that the angular positions of the equatorial reflections of the crystal and the mesophase are similar. The transition of the cellulose–NMMO system to the mesophase is probably related to the structural features of cellulose as a high-regular polymer with a developed system of H-bonds.

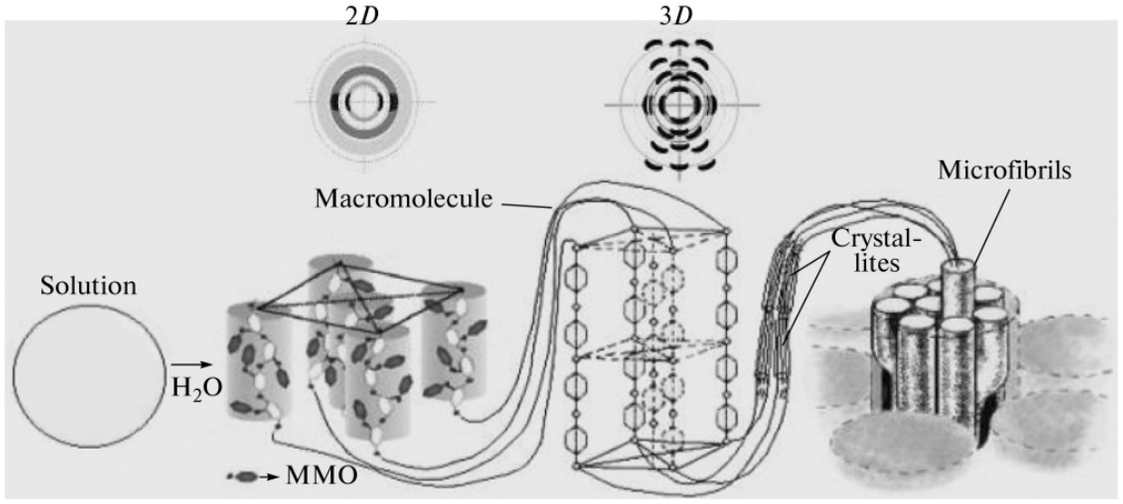

Figure 23. Schematic representation of the evolution in the cellulose structure during spinning of fiber samples from cellulose solutions in NMMO

Let us consider the evolution of the cellulose structure in blends. According to the X-ray data, all NMMO solutions of cellulose blended with copolyesters, PMPIA or clays, are amorphous; however, the character of structural transformations in them during isolation of the polymer phase is appreciably different from that in cellulose solutions [19]. Our experiments showed that although the chemical nature of the polymer introduced in cellulose solutions and the phase states and morphologies of blend solutions are different, the resultant structure of the formed blend polymer phase is of the same type. Since the evolution of the structure is the most pronounced for the cellulose–PMPIA system, let us examine step-by-step formation of the structure of cellulose composites.

After removal of the solvent, cellulose composites containing 5% PMPIA, as is seen from the diffractograms shown in Fig. 24, are not amorphous even in the absence of drawing, and demonstrate a marked increase in the intensity of scattering in the range of angles $2\theta = 12°$ in the equatorial direction and the absence of redistribution between equatorial and meridional scatterings at $2\theta > 15°$ (Figs. 24, 25a).

Presence of two peaks on the diffractogram indicates that the packing with two mean intermolecular spacings occurs. These spacings are appreciably different. It is quite probable that the molecules located in the closest proximity more easily form the system of inter- and intramolecular hydrogen bonds that is necessary for formation of ordered domains capable to be oriented. Therefore, the layered 1D packaging is formed at a small draw ratio ($\lambda = 6$) (Fig. 25a).

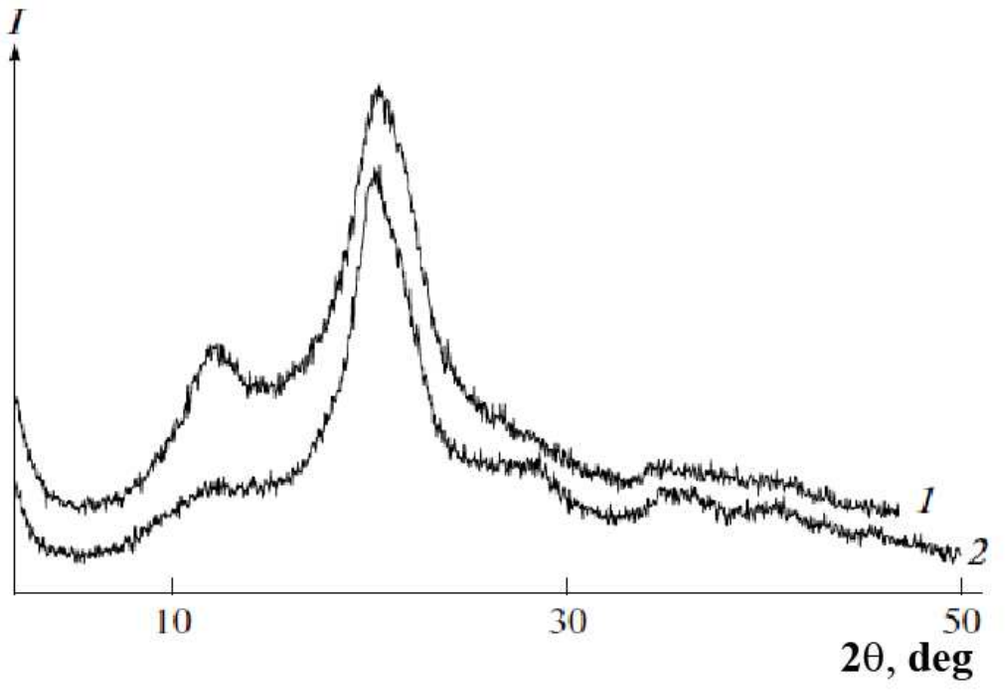

Figure 24. Equatorial (1) and meridional (2) diffractograms of blend extrudates composed of 95% cellulose and 5% PMPIA

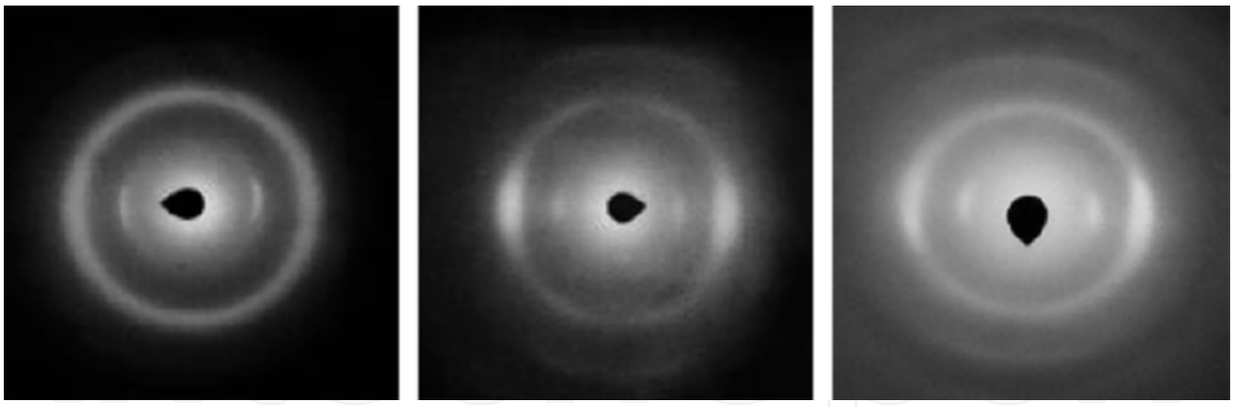

Figure 25. X-ray patterns of blend fiber samples composed of 95% cellulose and 5% PMPIA at various draw ratios: λ = (a) 6, (b) 13, and (c) 17.

Formation of composite fibers under conditions of orientation drawing accompanies by further evolution in the scattering pattern. As is seen from Fig. 25b, the redistribution of intensity covers now the entire region of scattering. As in the case of the purely cellulose mesomophic gel fiber, two reflections are observed on the equator (22 b). As the order of packing of cellulose macromolecules in the basal plane (at the intermolecular level) is improved, the transition of the layered 1D packing to the 2D columnar mesophase occurs. In this case, the position of equatorial reflections on the X-ray patterns of the oriented blend sample coincides with the position of equatorial reflections of the mesophase cellulose gel fiber and with the position of main basal reflection 101 of the cellulose crystal.

An increase in the draw ratio of the composite sample to λ = 17 facilitates further perfection of its structure. On the X-ray pattern of the fiber (Fig. 25c), the meridional reflection appears at 2θ =35°C. The features of scattering in the vicinity of the equator, which have been previous assigned to ordering in the basal plane, are preserved. At the same time, there are no reflections in the quadrants of the X-ray pattern.

A comparison of the oriented fibers of cellulose and the composite having the same draw ratios convincingly proves this finding. In fact, scanning of the composite fiber samples reveals no near-meridional reflections or other quadrant reflections (Fig. 26). The absence of quadrant reflections is the distinguishing feature of the composite fiber. At the same time, the angular positions and the half-widths of equatorial and meridional reflections for the cellulose and composite fibers are almost the same at a small content of the polymer additive (4%).

The above described picture of scattering obtained for the composite fiber with λ = 17 shows that the system contains two independent levels of order: 2D order in the basal plane (the intermolecular level) and 1D order along the fiber axis (the intramolecular level), that is, on the whole, non-crystalline 3D order. Fig. 27 schematically represents the most pronounced structural transformations occurring during isolation of the polymer phase from blend solutions in NMMO.

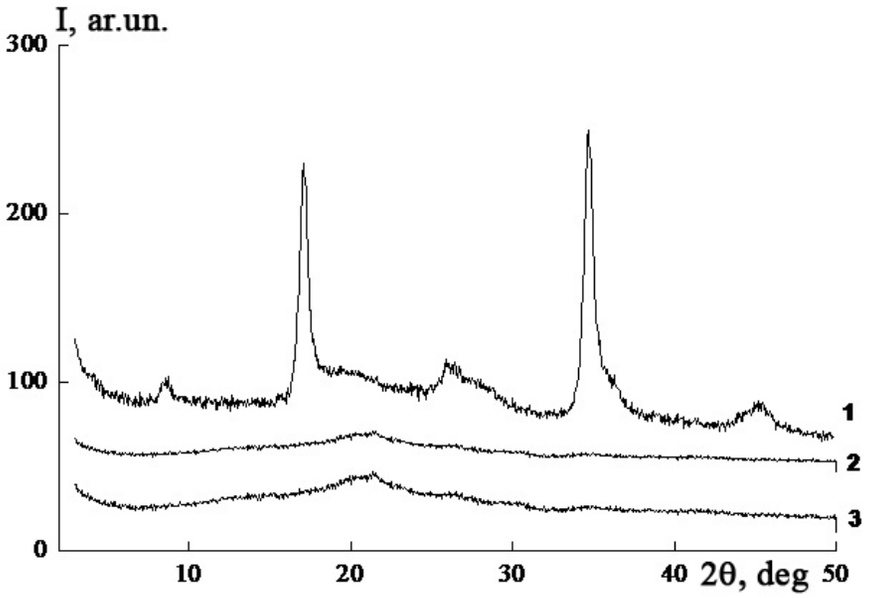

Figure 26. Diffractograms of the composite cellulose fiber containing 4% PMPIA during scanning (1) along the meridian and at angles to the meridian of (2) 10° and (3) 20°.

Thus, it has been shown for the first time that the introduction of copolyester and PMPIA into cellulose solutions in NMMO makes it possible to govern the processes of cellulose structuring and to stop them at the stage of formation of the 2D mesophase and, thus, to avoid further perfection of the structure and formation of the crystalline phase of cellulose.

On the basis of the above evidence, evolution in the structure of cellulose during isolation of the polymer phase from its own solutions and solutions of cellulose blends in NMMO may be depicted as follows. If the cellulose fiber is spun from NMMO solutions under the conditions of uniaxial drawing, the structure of cellulose forms in two stages. At the first stage, when the solvent is incompletely removed from solution (~95%) and, accordingly, the phase separation is incomplete, regular interchain periodicity develops in the main bulk of the cellulose phase. NMMO molecules remaining in the polymer phase are linked via strong electron donor–acceptor bonds with protons of hydroxyl groups of cellulose and, thus, favor restoration of intrachain hydrogen bonds that are necessary for the formation of classical three-dimensional ordering. As a consequence, conformational distortions appear in chains and only the two-dimensional ordering of the 2D mesophase type is implemented in the system. At the second stage, when the solvent is fully removed and, accordingly, when the phase decomposition in the cellulose phase is completed, the traditional ensemble of inter and intramolecular hydrogen bonds forms and cellulose passes to the crystalline phase.

Copolyester and PMPIA are thermodynamically incompatible with cellulose but possess high affinity for NMMO. These polymers dissolve in NMMO to form solutions that in the case of copolyester are compatible with the solution of cellulose. However, in the case of PMPIA, the inverse situation is observed: solutions of cellulose and PMPIA in the same

solvent are incompatible. During isolation of the polymer phase from blend solutions, the redistribution of specific interactions and hydrogen bonds, but conformational transformations of cellulose macromolecules associated with incompatibility of polymers most probably create steric hindrances to the development of intermolecular ordering that is traditional for cellulose.

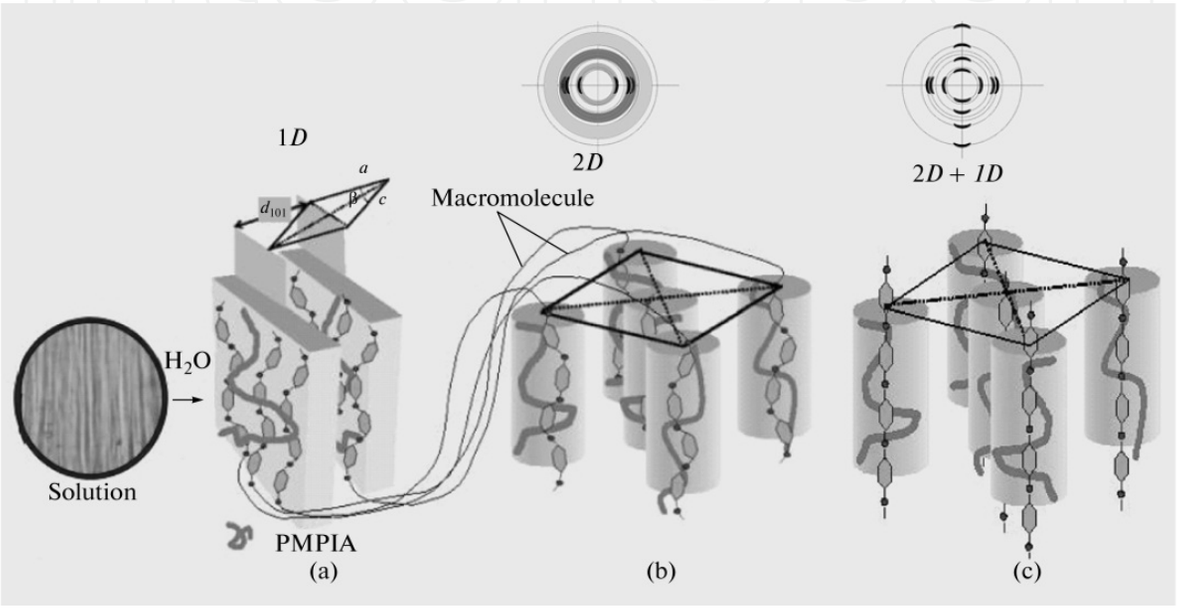

Figure 27. Schematic representation of the structure evolution during spinning of composite fibers from the cellulose–NMMO–

PMPIA blend system: (a) 1D order in the basal plane (layered, intermolecular); (b) 2D order in the basal plane (intermolecular); and (c) 2D order in the basal plane (intermolecular) + 1D order along the fiber axis (intramolecular), that is, →3D noncrystalline order.

5.2. Structure of cellulose and its blends with aluminosilicates

The evolution of structure transformations in composite systems based on cellulose and layered aluminosilicates Cloisite Na^+ and Cloisite 20Å, obtained through a stage of solid-phase dissolution of cellulose in NMMO, has been investigated by X-ray diffraction (XRD) technique [20-22]. A solid-phase process provides high dispersion and uniform distribution of particles of clay in a matrix cellulose phase.

Diffractograms in Fig.28 reflect interaction between components of the system "cellulose-Cloisite Na^+-NMMO" realized on the first stage of the process—the solid-state activation.

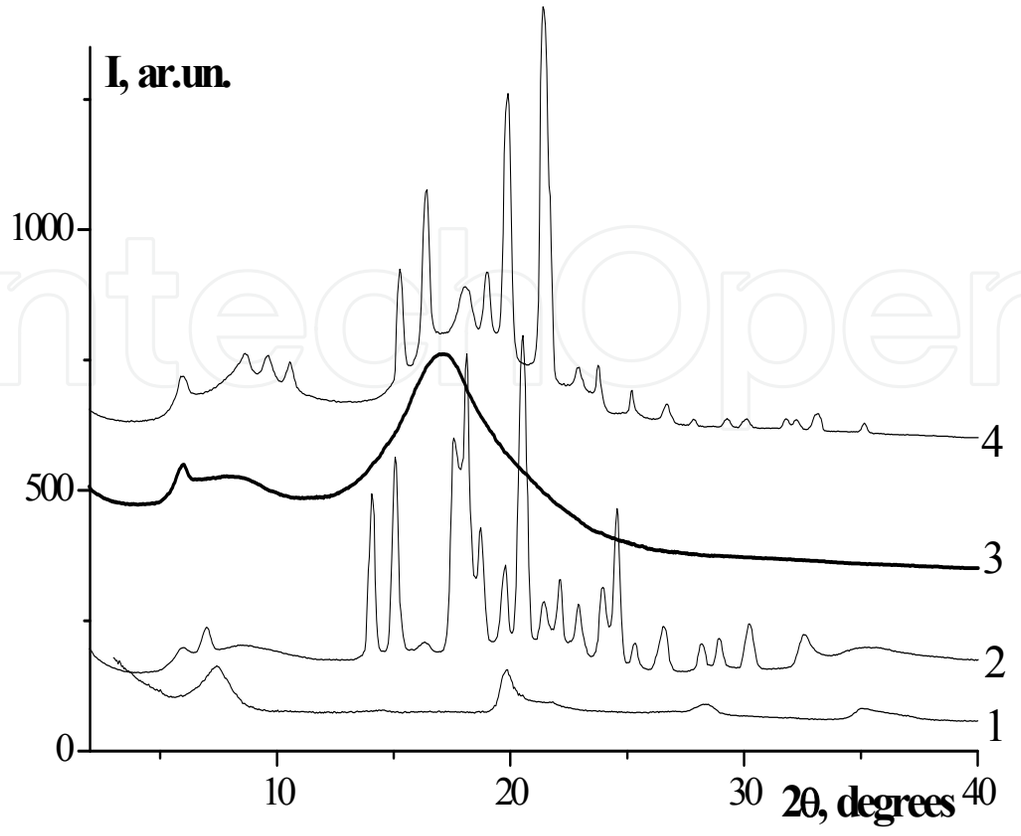

Figure 28. Diffractograms of Cloisite Na^+ (1), solid-activated mix system: 16,2% cellulose - 1,8% Cloisite Na^+ - 82% MMO at 20 (2), 120 (3) and 20°C after cooling from 120°C (4)

Comparison of the X-ray characteristics indicates that after introducing the clay into the composition no changes in the angular position of the basic layer peak of the clay at $2\theta_L$ take place. However, an additional peak appears shifted a little to a small-angle side in comparison with the reflection at $2\theta_L$. The shift of the additional new peak corresponds to the increase of interlayer spacing for 3 Å. This additional peak becomes the basic one on heating up to 120°C (curve 3) and subsequent cooling (curve 4). It seems that the weak changes in clay interlayer spacing are caused by water migration from the system to the clay due to their high affinity to each other. So, the XRD pattern of the solid-phase treated by composition corresponds to the superposition of the two patterns: Cloisite Na^+ and the solid pre-solution of cellulose in NMMO.

The scanning at a low speed with high acquisition reveals no reflexes in the angular region of $2\theta < 3°$, that did not enables us treat this system as an intercalated one.

Nanosize particles (M_2Cloisite Na^+), received as a result of activating dispersion of Cloisite Na^+, are discrete tacktoids with the same interlayer distance as in the initial clay. Possibly, such type of a clay structure is caused by steric restriction for the penetration of bulk H-complexes into interlayer regions of the polar montmorillonite Cloisite Na^+.

Essentially different structure of activated solid-phase mixed system is realized in Cloisite 20 A. As seen at the equatorial XRD pattern of the composition (Fig. 29), the basic layer peak

of Cloisite 20A shifts to the small-angle region from the initial angular position $2\theta_L$=3.3º to $2\theta_L$=1.76°, (curve 1).

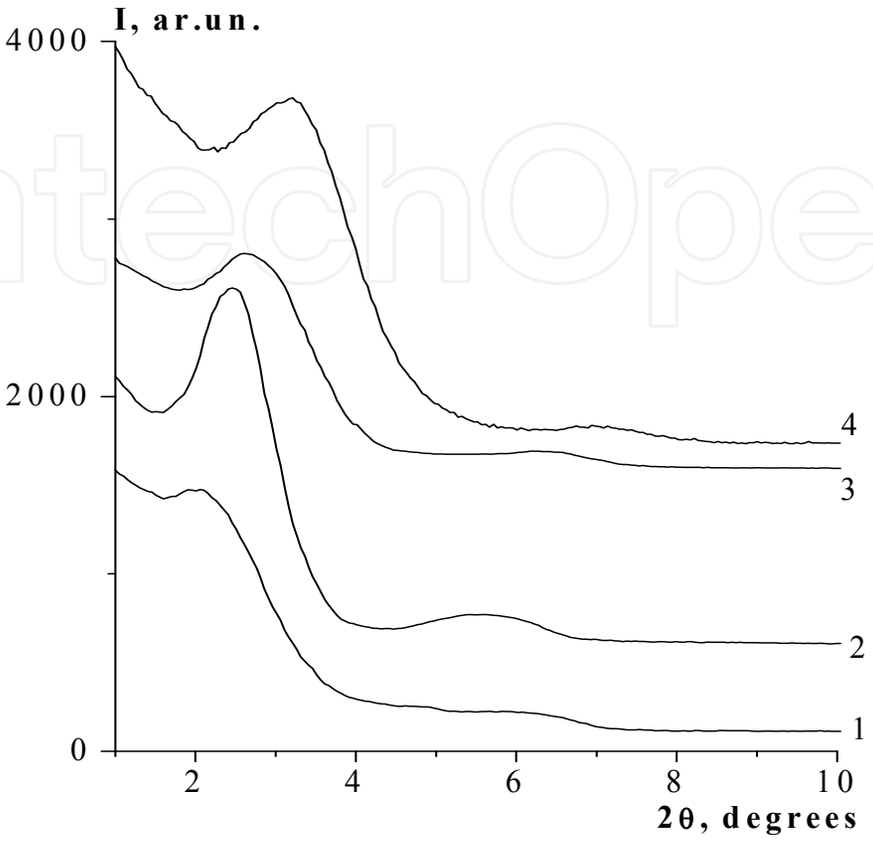

Figure 29. Diffractograms of the solid-phase activated system 16,2% cellulose-1,8% Cloisite 20A - 82% MMO at 20 (1), 120 (2), 20°C after cooling from 120°C (3) and Cloisite 20A (4).

That is caused by the influence of shear stress. Molecules of cellulose and NMMO penetrate into interlayer regions of the clay crystal lattice causing to the shift one-dimensional expansion by more than 20Å. It happens in spite of the hydrophobic nature of Cloisite 20A conditioned due to the presence of non-polar side modifying substituents. A heating and, accordingly, melting of mixed "solid" pre-solutions, they transfer into a viscous state that leads to the changes in the XRD pattern (curve 2): the intensity of the basic layer peak of the modified clay sharply increases and the angular position of this peak slightly shifts towards wide- angle side up to $2\theta_L$=2.04º. The similar changes in the character of the XRD pattern occur also on heating the individual Cloisite 20A. This is apparently connected with conformational changes of its side chains. Conformational reorganization happened on heating promotes the formation of more perfect and homogeneous structure also after cooling the sample. This manifests itself by the intensive growth of the peak at $2\theta_L$ (curve 3).

The above cited set of experimental data allows us to come to the following conclusions. Under the solid-phase activation of a cellulose-NMMO-Cloisite Na^+ system the solid-phase complex formation between molecules of cellulose and NMMO occurs only. As for the system cellulose-NMMO- Cloisite 20A, herein a reaction of solid-phase intercalation of

molecules of cellulose and NMMO into the interlayer regions of the modified clay happens alongside with processes of H-complex formation between cellulose and NMMO.

Under simultaneous influence of temperature and velocity gradient solid-phase pre-solutions melt and passes into a viscous state. As seen in Fig. 30, the XRD patterns of mixed solutions of cellulose in NMMO, containing Cloisite Na^+, are characterized by the slight shift of the basic layer peak of the clay towards the small-angle side, i.e. identically to what happens in solid-phase state.

Moreover, the basic layer peak of the clay at $2\theta_L$ is characterized by higher intensity on the equator in comparison with the meridian (Fig. 30). Such character of azimuthal redistribution of peak intensity is obliged to high-degree orientation of discrete clay particles along the flow axis direction. It is achieved under the influence of longitudinal and shear stresses arising in the pre-entered zone of a capillary. Schematic representation of the realized structure is presented in Fig. 30a.

The structures of the mixed solutions of cellulose in NMMO, containing Cloisite 20A, and the activated solid-phase compositions are completely identical and are characterized by pronounced intercalation of the cellulose macromolecules solvated by NMMO into interlayer regions of the clay.

The revealed structural peculiarities of the mixed systems under study demonstrate themselves the most essentially at the last stage of the process – allocation of a cellulose-silicate phase from NMMO solutions.

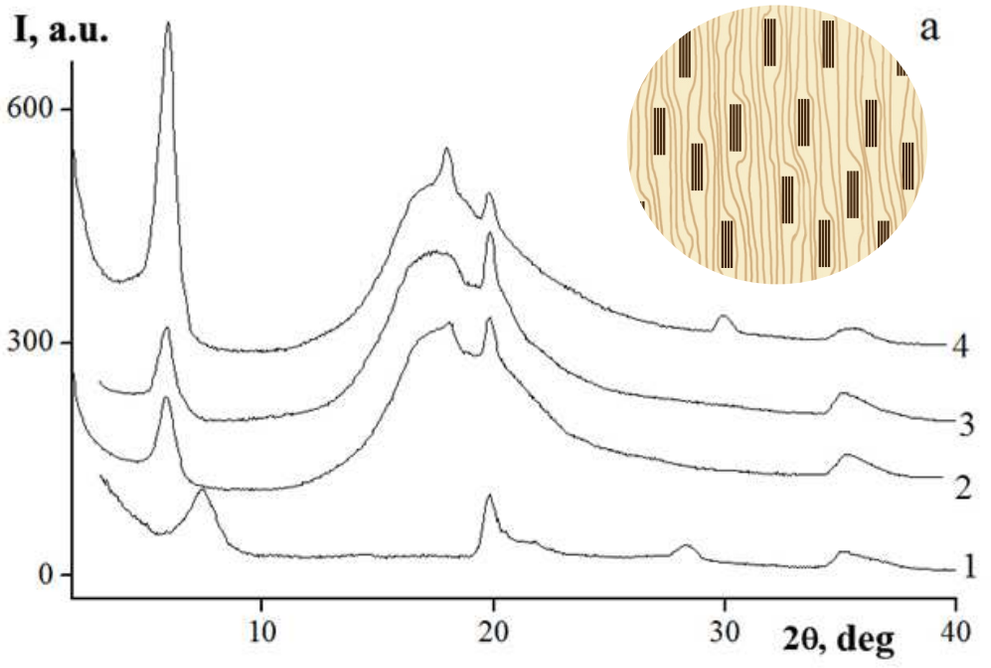

Figure 30. Diffractograms of Cloisite Na^+ (1), 18% cellulose solution in NMMO, containing 10% Cloisite Na^+, in film form (2), in extrudate form (3 – meridional, 4 – equatorial) and schematic representation of the solution extrudate structure (a).

The XRD patterns of oriented samples of the cellulose-Cloisite Na^+ compositions (Fig. 31) are characterized by the practically similar slight increase of the clay interlayer spacing d_L up to 15.0Å, like in the case of the activated solid-phase mixtures and solutions described ealier. Such a character of the XRD patterns is indicative of complete absence of intercalation.

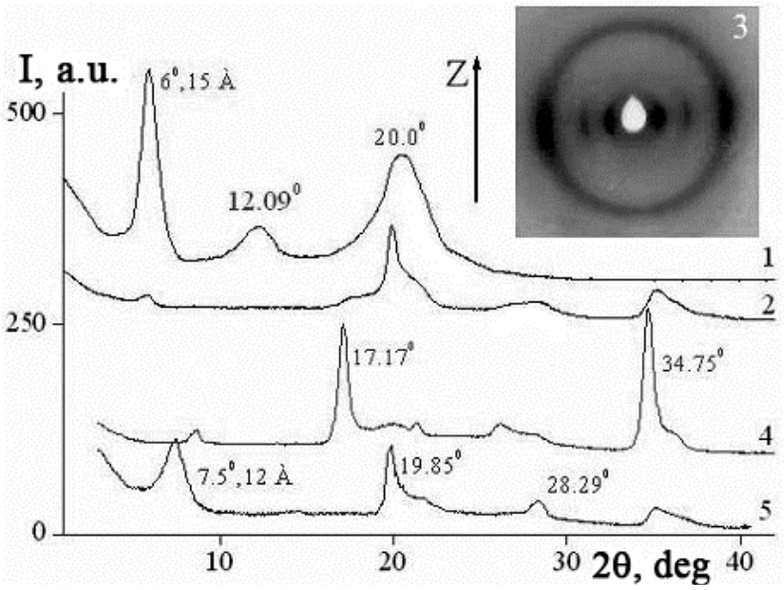

Figure 31. Equatorial (1) and meridional (2) diffractograms and X-ray pattents (3) of composite sample of 90% cellulose + 10% Cloisite Na^+; meridional diffractogram of cellulose fibers (4) powder diffractogram of Cloisite Na^+ (5).

Analysis of the X-ray patterns of oriented samples allows us to obtain more exact information about realized structure. So, two equatorial peaks rather legibly manifest themselves on the equator of pattern of a mixed sample (Fig. 31a). One of the peaks located in at wide angles corresponds to the oriented cellulose. The angular positions of the equatorial peaks of cellulose on the patterns for mixed system (Fig. 31a) and oriented cellulose partially washed-out from NMMO (22b) coincide. As has been mentioned above, the presence of only these equatorial peaks indicates that cellulose macromolecules form the columnar type 2D-mesophase. The peak of oriented clay is also present on the equator of the mixture pattern. Is has been also established that the degree of orientation for both components depends on a content of nanocomposites. The increase of content and, accordingly, the degree of structuredness of cellulose phase in solution promotes the rise of an orientation order for both, cellulose itself and clay. The X-ray patterns of composite with Cloisite 20A and composite of cellulose with Cloisite Na^+ as additive are practically identical.

Thus, a cellulose phase under the influence of shear stress is oriented and this initiates the implementation of certain orientational order of anizodiametric clay particles. The oriented clay particles give an additional impact on orienting the cellulose phase. In other words, in mixed solutions and respectively in the composites develop a unique synergy of orientation of the matrix phase and the filler. At the same time, particles of the clay immobilized in the matrix phase retain their size and do not aggregated.

Apparently, under the influence of shear of mixed systems at capillary flow anisodiametric solid particles of the filler embedding in a less structured region of the matrix phase, orient in the direction of extrusion. This leads to a perturbation of the stress and velocity fields of a viscoelastic matrix phase of cellulose and, consequently, to its local deformation. The stressed state of the matrix at the micro level does not allow the cellulose macromolecules rearrange with the formation a three-dimensional crystal structure. As a result, two-dimensional but not three-dimensional structure is formed, and it is characterized by a regular packing of conformationally disordered macromolecules of cellulose in the basal plane. Schematic representation of the evolution in the cellulose structure during spinning of fiber samples from mixed solutions of cellulose in NMMO with the addition of nanoparticles of clay is presented in Fig. 32.

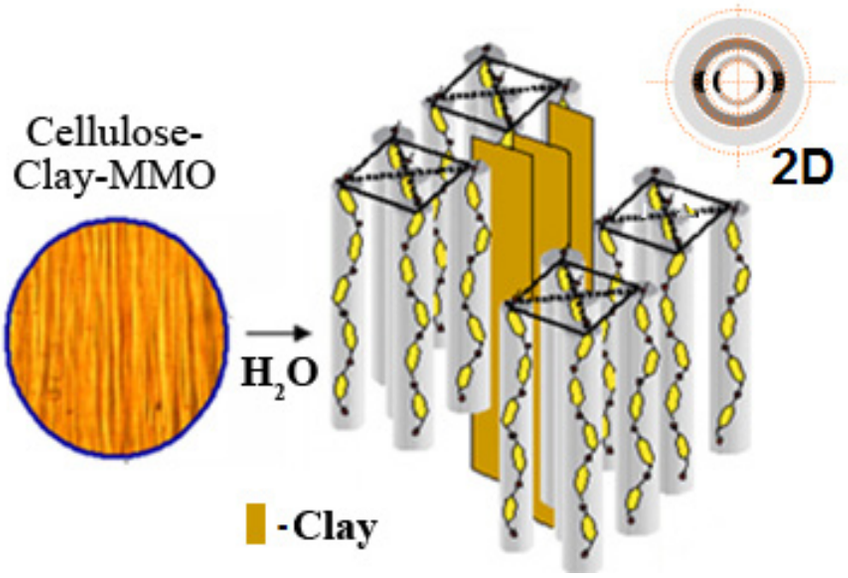

Figure 32. Schematic representation of the structure evolution during spinning of composite fibers from the cellulose–clay–NMMO blend system.

So, it has been shown that the introduction of copolyester, PMPIA and clays into cellulose solutions in NMMO makes it possible to govern the processes of the cellulose structuring and to finish them on the stage of the 2*D* mesophase formation and, thus, to avoid further perfection of the structure and the formation of the crystalline phase of cellulose. In other words, the structural situation is the same as in the case of the as-spun cellulose fibers. The only difference is that, in purely cellulose fibers, the resulting mesophase is not at equilibrium, while in blend systems, the 2*D* mesophase forms after the complete phase decomposition of the system and, correspondingly, is at equilibrium.

6. Fibrillization and mechanical properties of cellulose and synthetic polymers and layered aluminosilicates micro- and nanocomposite fibers

The following structure peculiarity of the process under discussion was found. This is the formation of mesamorphic matrix cellulose phase due to introducing synthetic polymers or

micro- and nanoadditives of layers alumonosilicates into cellulose solutions. This effect allows us to solve two important concerns of the processing of cellulose from solution in NMMO: it prevents fibers fibrillation and provides high mechanical properties of novel composite materials. Photomicrographs of cellulose and mixed fibers obtained before and after vibrating mill treatment are shown in Fig. 33.

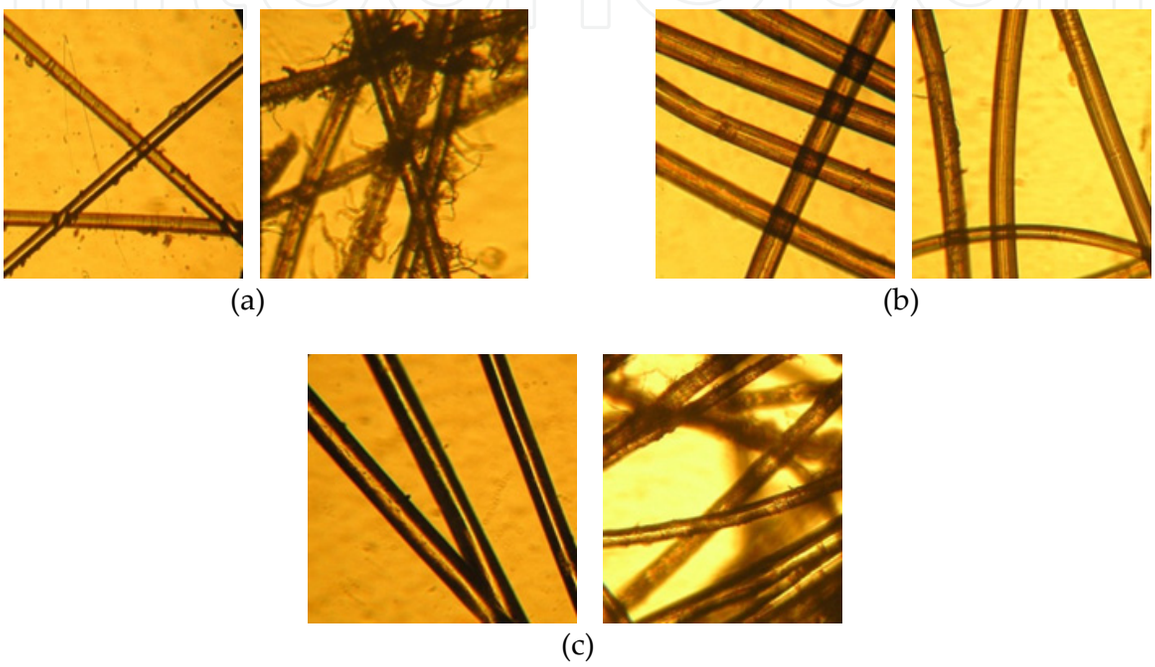

Figure 33. Micrographs of cellulose (a) and mixed fibers: cellulose/PMPIA (b) and cellulose/M_2CloisiteNa$^+$(c) before and after mechanical treatment in a vibrating mill in the aquatic environment (diameter of the fibers is 14-16 μm).

The obtained micro- and nanocomposite fiber cellulose/CPE (PMPIA) and cellulose/clay have high mechanical properties, which by 1.5–3 times exceed the strength properties of cellulose fibers (Table1). At the same time, the deformation parameters of composite fibers are not reduced, and, in some cases, are substantially increased in comparison with the standard cellulose fibers.

System	*Ø*, μm	s,MPa	*ε*, %	*E, GPa*
Cellulose 100 %	34	420	10	11
Cellulose 95% - PMPIA 5%	28	710	12	22,6
Cellulose 90% – Cloisite Na$^+$ 10%	30	530	11	14
Cellulose 99,97% – Cloisite Na$^+$ 0,03%	18	1520	10	30

Table 1. Mechanical properties of micro- and nanocomposites

7. Conclusion

A method for the preparation of solid-phase compositions of cellulose with synthetic polymers and layered aluminosilicates Cloisite Na^+ and Cloisite 20A has been developed. It provides high dispersion and uniform distribution of a polymer or micro- and clay nanoparticles in the matrix cellulose phase.

The addition of polymers and clay to cellulose solutions in NMMO, regardless of the nature of a polymer as well as phase and/or structure peculiarities of mixed solutions, allows us to control the process of structurization of the matrix cellulose phase, leading it to the formation of 2D mesophase, thereby excluding a possibility of crystallization.

Novel nanostructures composed of cellulose/clay and cellulose/polymer fibers possess high mechanical properties: their strength and modulus are 1,5–2 times higher than those of cellulose.

Our studies have made it possible to approach the solution of an extremely important issue that consists in the regulation of the cellulose structuring. Until now this did not have any direct solution. Thus, it becomes possible to manufacture cellulose-based fibers that have the desired combination of characteristics.

Author details

Ludmila Golova, Igor Makarov, Ludmila Kuznetsova,
Elena Plotnikova and Valery Kulichikhin
A.V. Topchiev Institute of Petrochemical Synthesis, Russian Academy of Sciences, Moscow, Russia

8. References

[1] Franks N. F. and Varga J. K. 1979, US Patent, No. 4290815
[2] Chanzy H., Noe P., Paillet M., Smith P. Swelling and dissolution of cellulose in amine oxide/water systems. Journal of Applied Polymer Science: Applied Polymer Symposium 1983; 37 239-259.
[3] Kruger R. Cellulosic filament yarn from the NMMO process. Lenzinger Berichte 1994; 4 49-52.
[4] Golova L. K., Kulichikhin V. G., and Papkov S. P. Mexanism of dissolution of cellulose in nonaqueous solvents. Vysokomol. Soedin 1986; A(28) 1795-2016.
[5] Cousey H. A., Smith S.B. The Formation and Structure of a new Cellulose Fibre. Lenzinger Bericht 1996; 7 51-63.
[6] Golova L. K. 1992, Russia Patent, No. 1645308
[7] Golova L. K. A new method of processing cellulose via highly concentrated “solid solutions”. Khim. Volokna 1996; 1 13-21.

[8] Golova L. K., Makarov I. S., Matukhina E. V., Kuptsov S. A., Shambilova G. K. and Kulichikhin V. G. Crystal Solvates of Thermotropic Alkylenearomatic Copolyesters and Poly(*m*-phenyleneisophthalamide) with *N*-Methylmorpholine-*N*-oxide . Vysokomol.Soedin 2008; A (50) 665 – 678.

[9] Amstrong R.N., Varga J.K., McCorsley C.C. Spinnable solutions of cellulose dissolved in amine oxides. Proceeding of the Fifth International Tappi Dissolving Pulp Conference, Vienna; 1980.

[10] Chanzy H., Dube V., Marchessault R.H. Crystallization of cellulose with NMMO: a new method a texturing cellulose. Journal of Polymer Science: Polymer Letters Edition 1979; 17 (4) 219-226.

[11] Golova L. K., Borodina O. E., Kuznetsova L. K. Hard Phase MMO-Process. Khim. Volokna 2000; 4 14-21.

[12] Papkov S. P. Physicochemical Principles of Polymer Solution Processing. Khimiya, Moscow. Russian; 1971.

[13] Weigel P., Gensrich J., Fink H.P. The structural format of cellulose fibres from amine oxide solutions. Lenzinger Berichte 1994; 9 35-41.

[14] Makarov I.S., Golova L.K., Plotnikova E. P., Matukhina E.V., Rebrov A.V., Kulichikhin V.G. RHEOLOGICAL PROPERTIES AND STRUCTURE OF NANOCOMPOSITES BASED ON CELLULOSE WITH NA-MONTMORILLONITE. 2nd International Polysaccharide Conference. Wageningen – Holland; 2011.

[15] Plotnikova E. P., Golova L.K., Makarov I.S., Kulichikhin V.G.Rheological properties of solutions of cellulose containing particles of aluminum silicates in MMO. Vysokomol.Soedin; 2012. (in press).

[16] Schurz J., Lenz J. Investigations on the structure of regenerated cellulose fibrer. Macromol. Symp. 1994; 83 273-289.

[17] Andersen E.M., Mitchell G.R. In Situ X-ray scattering investigation of solution of cellulose in NMMO during shear flow. Polymer 1998; 39 (26) 7127-7129.

[18] Golova L. K., Makarov I. S., Plotnikova E. P., Tereshin A. K, and Kulichikhin V. G. Solutions of Mixtures of Cellulose and Synthetic Polymers in *N*-methylmorpholine-*N*-oxide,Polymer Science . Vysokomol.Soedin 2009; A (51) 414-420.

[19] Golova L. K., Makarov I. S., E Matukhina E.V., Kulichikhin V.G. Solutions of Cellulose and Its Blends with Synthetic Polymers in N- Methylmorpholine-N-oxide: Preparation, Phase State, Structure, and Properties . Vysokomol.Soedin. 2010; A 52(11) 1209-1219.

[20] Makarov I.S., Golova L.K., Matukhina E.V., Kulichikhin V.G. Cellulose nano- and microcomposites with natural and modified clays. 10th Annual Conference, YUCOMAT Herceg Novi, Montenegro; 2008.

[21] Makarov I.S., Golova L.K., Matukhina E.V., Kulichikhin V.G. Biodegradable composite materials on the basis of cellulose with synthetic polymers and laminated aluminosilicates. The 1st EPNOE Conference "Polysaccharides as a Source of Advanced Materials".Turku, Finland; 2009.

[22] Makarov I.S., Golova L.K., Rebrov A.V., Matukhina E.V., Kulichikhin V.G. Biodegrable nanocomposites based on cellulose with Na-montmorillonite. AERC 2011. 7th Annual European Rheology Conference .Suzdal - Russia; 2011.

IntechOpen